An Alternative Homodimerization Interface of MnmG Reveals a Conformational Dynamics that Is Essential for Its tRNA Modification Function

Rafael Ruiz-Partida [1], Silvia Prado [1], Magda Villarroya [1], Adrián Velázquez-Campoy [2,3,4,5], Jerónimo Bravo [6] and M.-Eugenia Armengod [1,7],

*1 - **Centro de Investigación Príncipe Felipe,** Valencia 46012, Spain*
*2 - **Institute of Biocomputation and Physics of Complex Systems (BIFI),** Joint Units IQFR-CSIC-BIFI, and GBsC-CSIC-BIFI, and Department of Biochemistry and Molecular and Cell Biology, Universidad de Zaragoza, Zaragoza 50018, Spain*
*3 - **Aragon Institute for Health Research (IIS Aragon),** Zaragoza, 50009, Spain*
*4 - **Biomedical Research Networking Centre for Liver and Digestive Diseases (CIBERehd),** Madrid 28029, Spain*
*5 - **Fundacion ARAID,** Government of Aragon, Zaragoza 50018, Spain*
*6 - **Instituto de Biomedicina de Valencia-CSIC,** Valencia 46010, Spain*
*7 - **Biomedical Research Networking Centre for Rare Diseases (CIBERER,** Node 721), Valencia, Spain*

***Correspondence to Rafael Ruiz-Partida and M.-Eugenia Armengod:** Centro de Investigación Príncipe Felipe, Valencia 46012, Spain. rnamod@cipf.es; marmengod@cipf.es*
https://doi.org/10.1016/j.jmb.2018.05.035
Edited by Dan Tawfik

Abstract

The *Escherichia coli* homodimeric proteins MnmE and MnmG form a functional complex, MnmEG, that modifies tRNAs using GTP, methylene-tetrahydrofolate, FAD, and glycine or ammonium. MnmE is a tetrahydrofolate- and GTP-binding protein, whereas MnmG is a FAD-binding protein with each protomer composed of the FAD-binding domain, two insertion domains, and the helical C-terminal domain. The detailed mechanism of the MnmEG-mediated reaction remains unclear partially due to incomplete structural information on the free- and substrate-bound forms of the complex. In this study, we show that MnmG can adopt in solution a dimer arrangement (form I) different from that currently considered as the only biologically active (form II). Normal mode analysis indicates that form I can oscillate in a range of open and closed conformations. Using isothermal titration calorimetry and native red electrophoresis, we show that a form-I open conformation, which can be stabilized *in vitro* by the formation of an interprotomer disulfide bond between the catalytic C277 residues, appears to be involved in the assembly of the MnmEG catalytic center. We also show that residues R196, D253, R436, R554 and E585 are important for the stabilization of form I and the tRNA modification function. We propose that the form I dynamics regulates the alternative access of MnmE and tRNA to the MnmG FAD active site. Finally, we show that the C-terminal region of MnmG contains a sterile alpha motif domain responsible for tRNA–protein and protein–protein interactions.

Introduction

tRNAs play a central role in protein translation and are, therefore, required for cell survival. In addition, tRNAs are involved in other important biological processes such as cell signaling and adaptive translation [1–3]. Post-transcriptional modifications of tRNAs, which are introduced by enzymes highly specific for tRNA species and positions, optimize the tRNA functions. In particular, wobble uridine (U34) modifications like those mediated by the Elongator complex (in cytosolic tRNAs) and the *Escherichia coli* MnmE and MnmG proteins and their eukaryotic homologs (in bacterial and mitochondrial tRNAs, respectively) are critical for efficient translation [4–8] and contribute to regulate global protein expression [2,3,7,9–11].

MnmE and MnmG are homodimeric proteins and form a complex, MnmEG, in which both proteins are functionally interdependent [12–14]. MnmEG catalyzes the synthesis of aminomethyl-uridine derivatives on U34 of $tRNA^{Lys}_{mnm5s2UUU}$, $tRNA^{Glu}_{mnm5s2UUC}$,

$tRNA^{Gln}_{(c)mnm5s2UUG}$, $tRNA^{Leu}_{cmnm5UmAA}$, $tRNA^{Arg}_{mnm5UCU}$ and $tRNA^{Gly}_{mnm5UCC}$ [14,15]. Lack of these modifications alters the relative efficiency of anticodons in reading cognate codons, causes translational frameshifting and produces a pleiotropic phenotype [4,16]. Notably, MnmE and MnmG have been included into the minimalist set of essential proteins required for the biogenesis of a functional translation apparatus in bacteria [17–19]. In humans, the MnmE and MnmG homologs, namely, GTPBP3 and MTO1, respectively, modify U34 in a set of mitochondrial tRNAs [20–22]. Defects in GTPBP3 and MTO1 affect mitochondrial translation, impair mitochondrial oxidative phosphorylation and cause infantile hypertrophic cardiomyopathy with lactic acidosis [20–26].

MnmE is a tetrahydrofolate- (THF-) and GTP-binding protein with each protomer (50 kDa) consisting of three domains: an N-terminal domain responsible for constitutive dimerization and the binding of THF; a central helical domain formed by residues from the middle and the C-terminal regions; and a GTP-binding domain (G-domain) with the canonical Ras-like fold (Fig. 1a and b, top), which is distantly located to the THF-binding domain [27,28].

MnmG is a FAD- and NADH-binding protein [13,29]. The structure of MnmG from *Aquifex aeolicus* (AaMnmG) was determined at 3.2 Å (form I, PDB ID: 2ZXH) and 2.3 Å (form II, PDB ID: 2ZXI) resolutions [30,31] and was found to be similar to those of MnmG from *E. coli* (EcMnmG, PDB IDs: 3CES and 3CP2) and *Chlorobium tepidum* (CtMnmG, PDB ID: 3CP8) [29,32]. Each MnmG protomer (69 kDa) is composed of the FAD-binding domain, the insertion domain 1 (Ins-1), the insertion domain 2 (Ins-2) and the helical C-terminal domain [29,31,32] (Fig. 1a and b, bottom). The AaMnmG structures, unlike those of EcMnmG and CtMnmG, revealed the tight interaction of MnmG with FAD, thus providing more detailed information on the active site of MnmG. In this work, the AaMnmG structures are used throughout and, in relation to the residue numbering, two numbers for each residue are provided in the text, the first referring to *E. coli* and the second to *A. aeolicus*, unless mentioned otherwise.

The asymmetric units of the AaMnmG form II, CtMnmG and EcMnmG crystals contain two homodimers in the classical "M-shaped" form [29,31,32]. The dimerization interface in all these cases is stabilized by well-conserved interactions between residues from the FAD domain on one protomer and residues from Ins-2 of the other (Fig. 1a, bottom). The asymmetric unit of the AaMnmG form I crystal contains two subunits connected through an alternative interface, but the classical M-shaped dimer can also be formed by crystal symmetry operations [31]. Therefore, the most predominant M-shaped dimer (form II) has been considered the physiologically relevant form of MnmG and, consequently, the only one used for the construction of the MnmEG models so far [29,33–35].

The EcMnmEG complex catalyzes *in vitro* the addition of the aminomethyl and carboxymethylaminomethyl (cmnm) groups at position 5 of U34 using ammonium and glycine, respectively [14] (Supplementary Fig. S1). Both reactions require GTP, FAD, and methylene-THF, which serves as the donor of the methylene carbon bonded directly to the C5 atom of the pyrimidine ring. The GTPase cycle of MnmE does not participate directly in the modification reaction. Rather, it is thought to orchestrate the reaction by inducing conformational changes relayed through MnmE and MnmG [27,28,33–39]. In contrast, it is assumed that the THF-binding domain of MnmE should be located close to the FAD-active site of MnmG in order to construct the catalytic center of the MnmEG complex [14,29,33]. Nevertheless, the detailed chemistry of the reaction and the overall architecture of the complex are currently unknown.

In this study, we show that the EcMnmG dimer adopts in solution the dimerization interface exhibited by the AaMnmG form I crystal structure, which, according to normal mode analyses, oscillates between open and closed conformations. We also show that a form-I open conformation is crucial for the binding of the dimeric THF-binding domain of EcMnmE to the FAD active center of EcMnmG. We propose a form I-based model for the assembly of the EcMnmEG complex whereby two identical and symmetrical catalytic centers are simultaneously generated. Finally, we show that the C-terminal region of EcMnmG contains a sterile alpha motif (SAM) domain, which is able to bind to tRNA and protein molecules.

Results

A dual role for the EcMnmG C_{ARM} in protein–protein interactions

In MnmG, the FAD-binding and insertion domains are forming a core (hereafter named catalytic core) from which the helical domain protrudes (Fig. 1a, bottom). Notably, the helical domain includes a highly conserved C-terminal region (hereafter, C_{ARM}), and a poorly conserved N-terminal region (hereafter, N_{ARM}) (Fig. 1b, bottom, and Supplementary Fig. S2). The relevance of the EcMnmG C_{ARM} for the interaction with EcMnmE has been previously reported [32,34]. On the basis of the EcMnmG and CtMnmG structures, which adopt the form II conformation, two highly conserved residues of the EcMnmG C_{ARM}, E585(579) and K589 (583), were proposed to be involved in the interaction with EcMnmE from gel filtration data on alanine mutants [29]. However, we found that the change of E585(579) (Fig. 1a, bottom) to lysine or alanine did not affect the EcMnmG-EcMnmE interaction in a surface plasmon resonance analysis, while impairing the tRNA modification function in an *in vivo* assay [32]. Thus, the role of E585(579) was unclear.

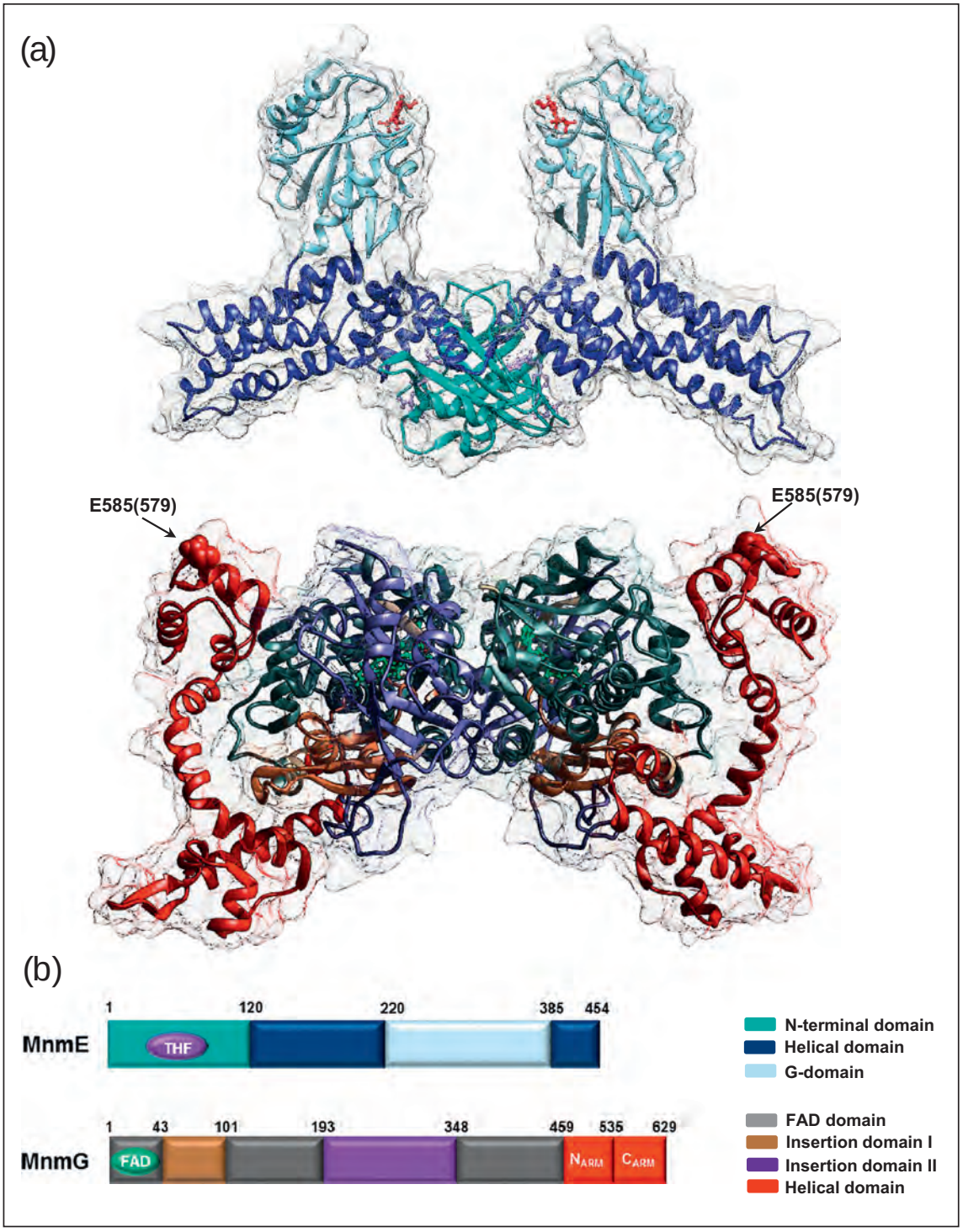

Fig. 1. Structures of MnmE and MnmG. (a) Ribbon representation of the crystal structures of CtMnmE (PDB ID: 3GEE; top panel) and the AaMnmG form II (PDB ID: 2ZXI; lower panel), colored as specified in panel b. Residue E585(579) selected in this study is shown in spheres. (b) Linear domain composition of EcMnmE and EcMnmG (*E. coli* numbering).

In the course of this work, we noted that in the AaMnmG form I (PDB ID 2ZXH), but not in form II (PDB ID 2ZXI), the C_{ARM} of one protomer interacts with the MnmG catalytic core of the other protomer, and that residue E585(579) is at hydrogen-bond distance from the strictly conserved R196(197) located in the Ins-2 domain of the opposite protomer (Fig. 2). Thus, E585 (579) could play a role in the stabilization of form I conformation. Then, we made additional observations: 1) structural information on MnmG revealed increased

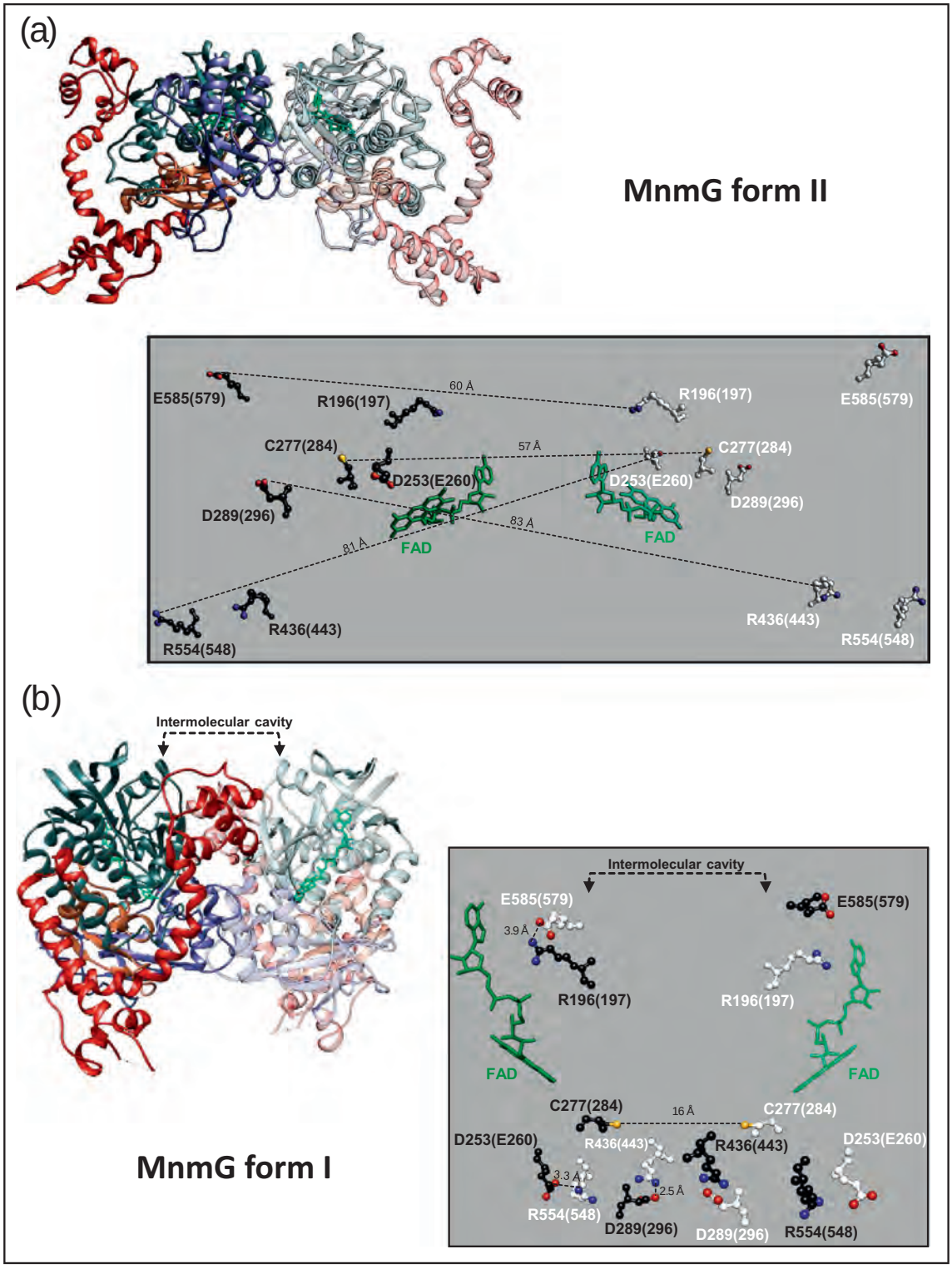

Fig. 2. Forms I and II of AaMnmG exhibit different dimerization interfaces. Ribbon representation of crystal structures of the AaMnmG form II (a) and the AaMnmG form I (b) colored in function of their domains as in Fig. 1. Residues highlighted in this study are represented in balls and sticks and colored in dark or white in function of the protomer where they are located (gray panels).

B-factors in the C_{ARM}, which suggests that this region could be more flexible than the rest of the protein; 2) normal mode analysis (NMA) of the AaMnmG protomer using *elNémo* and iMODS [40,41] indicated a concerted mobility of the C_{ARM} with respect to the catalytic core (Fig. 3); 3) an assembly analysis of both form I (PDB ID 2ZXH) and II (PDB ID 2ZXI) using PDBePISA [42] yielded a buried area of 7630Å^2 with a ΔG^{int} of −27.6 kcal/mol and a ΔG^{diss} of 10 kcal/mol for form II, whereas values of 8360 Å^2,

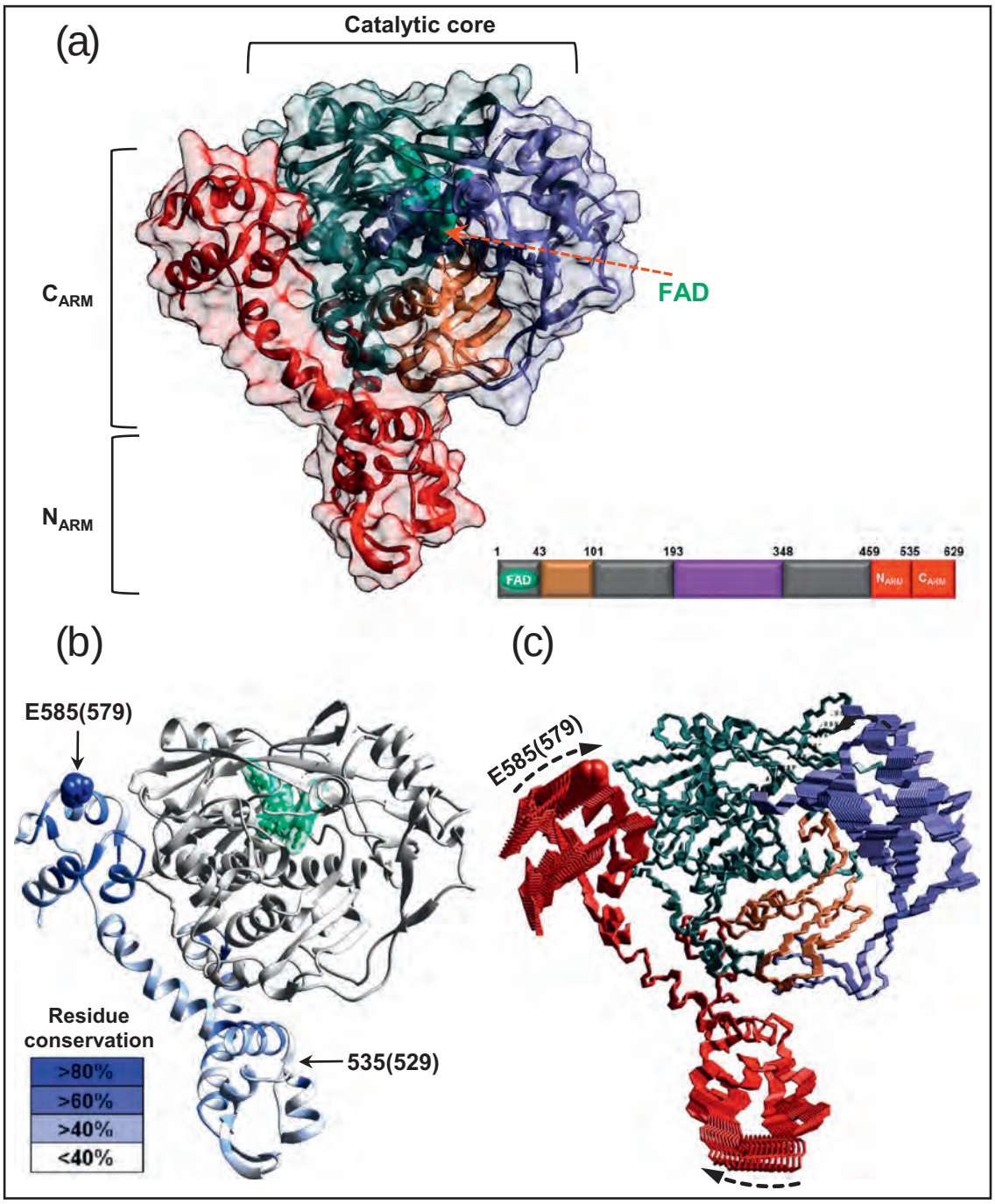

Fig. 3. The flexible MnmG C_{ARM} region. (a) Surface and ribbon representation of the AaMnmG form II protomer. (b) Ribbon representation of the AaMnmG form II protomer with the helical domain colored according to conservation score. Residue E585 (579) selected in this study is shown in spheres. Residue 535(529) marks the separation between C_{ARM} and N_{ARM}. FAD is shown in green. (c) Backbone representation of the models generated in the NMA analysis of AaMnmG form II protomer by *elNémo* server. Dashed arrows indicate the direction of the trajectories.

ΔG^{int} = −57.1 kcal/mol and ΔG^{diss} = 19.7 kcal/mol were obtained for form I; the slightly larger buried surface and the difference in the free energy of assembly dissociation suggest, at least, an assembly in the form I thermodynamically as stable as form II; 4) the form I contains a higher number of evolutionarily conserved residues involved in the dimerization interface than form II (Fig. 4 and Supplementary Fig. S2).

From all these data, we hypothesized that the form I may represent a physiological dimer, and that the C_{ARM} could be subjected to conformational rearrangements allowing the interaction with the MnmG catalytic core through the E585(579)-containing face. Several approaches were taken to test this hypothesis, which are summarized in Supplementary Fig. S3.

We first cloned the EcMnmG fragment from position 535 to 629, which includes the C_{ARM} (Fig. 1b, bottom), in an expression vector. The construct produced a soluble, highly pure, and α-helical polypeptide, EcMnmG(535–629), according to SDS-PAGE analysis and the circular dichroism spectra (Supplementary Fig. S4). By using isothermal titration calorimetry (ITC;

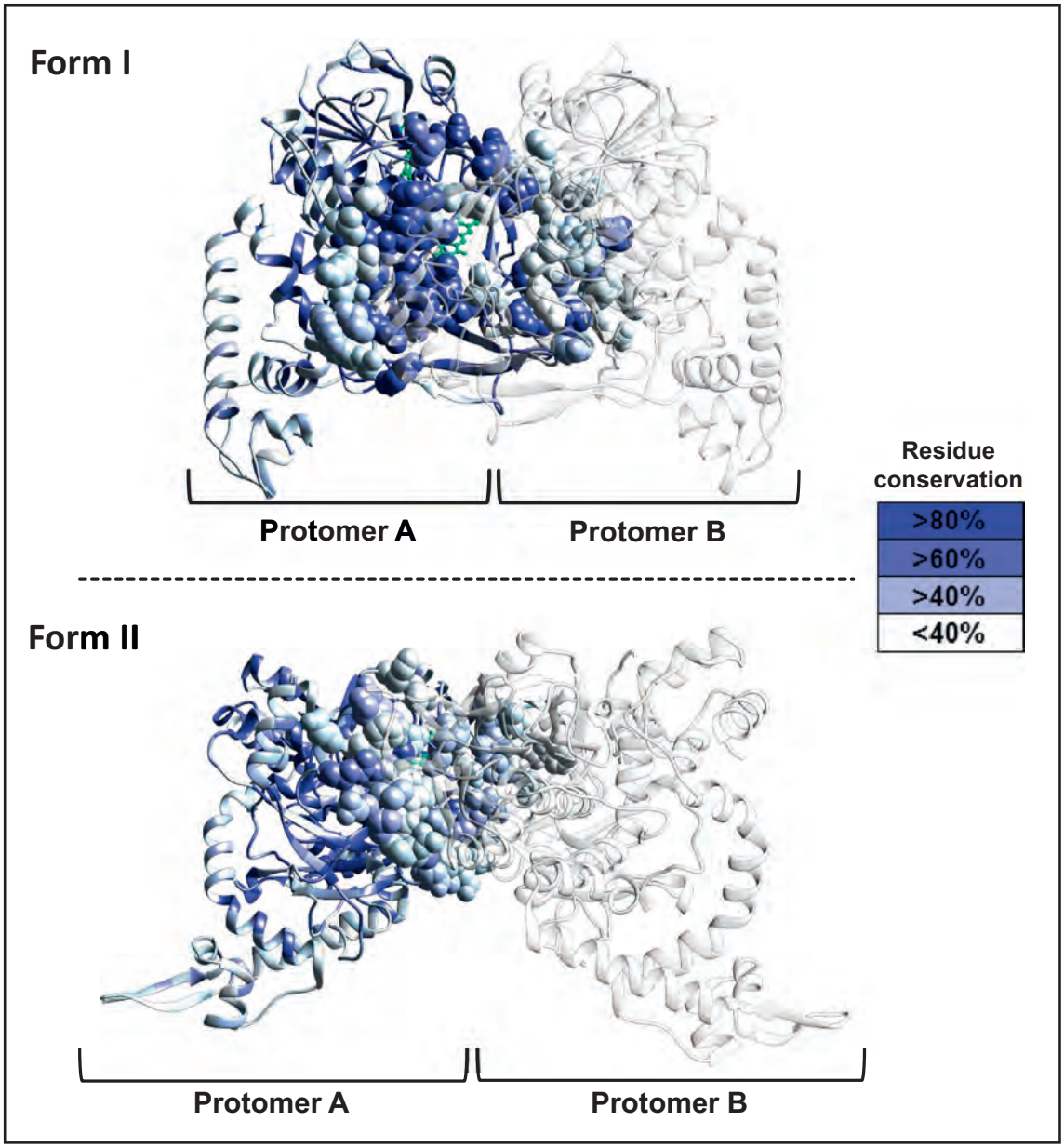

Fig. 4. Evolutionary conservation of residues in the dimerization interfaces of the MnmG forms I and II. Ribbon representation of the MnmG form I (top panel) and form II (bottom panel) rendered by residue conservation (inset). The residues of the protomer A that form part of the dimerization interface are represented in spheres. The secondary structure of the protomer B appears as partially transparent for visualization of the highlighted residues.

Table 1 and Supplementary Fig. S5), we found that the truncated variant EcMnmG(535–629) was able to interact with both the C-terminally truncated EcMnmG(1–550) protein (K_d = 1 μM) and EcMnmE (K_d = 25 μM). Notably, the presence of the E585K change in the EcMnmG(535–629) variant reduced its affinity for EcMnmG(1–550) by about 20-fold (K_d = 21 μM), whereas the interaction with EcMnmE was not affected (K_d = 24 μM), which suggests that E585K does not alter significantly the fold of MnmG(535–629). Altogether these data support the idea that E585 is involved in the interaction of EcMnmG(535–629) (i.e., the C_{ARM}) with the EcMnmG catalytic core, but not with EcMnmE. Interestingly, protein EcMnmG–E585K migrated slower than the wild-type protein in native red electrophoresis (NRE) [43], suggesting that the mutant full-length protein has a more expanded conformation than EcMnmG (Fig. 5a and b). This could be due to breakage of the salt bridge that E585(579) can form with residue R196(197) of the other protomer (Fig. 2). Moreover, considering that the E585K replacement reduced significantly the tRNA modification activity of EcMnmG *in vivo* (Table 2), we concluded that the interaction of the C_{ARM} with the MnmG catalytic core, which only occurs if EcMnmG adopts the form I conformation (Fig. 2), is biologically relevant.

This proposal was further supported by the finding that changes in other residues involved in the interaction between the C_{ARM} and the MnmG catalytic core in the form I conformation, like R554(548), D253 (E260) and R196(197) (see Fig. 2 and Supplementary Fig. S6), also reduced both the affinity between the EcMnmG(1–550) and EcMnmG(535–629) proteins (Table 1) as well as the tRNA modification function of the full-length protein (Table 2). Indeed, mutations R554D and D253R in, respectively, EcMnmG (535–629) and EcMnmG(1–550) led to a ≥20-fold decrease in affinity (K_d values of 34 and 26 μM; compared with K_d = 1 μM), whereas no binding was detected between EcMnmG(1–550)R196D and EcMnmG(535–629). Therefore, it is plausible that pairs E585(579)–R196(197) and R554(548)–D253 (E260) form intermolecular salt bridges important to maintain the interaction of the C_{ARM} with the MnmG catalytic core (Fig. 2 and Supplementary Fig. S6). Notably, in the context of full-length MnmG, variants E585K, R554D, D253R and R196D produced a null-like phenotype with respect to tRNA modification when expressed to wild-type levels (Table 2 and Supplementary Figs. S7 and S8). Forced overexpression of the mutant proteins produced complementation of the tRNA modification function (Table 2 and Supplementary Figs. S7 and S8). In contrast, the wild-type phenotype was not recovered after overexpression of EcMnmG-C277S, used here as a negative control (Table 2), which indicates that the change of the catalytic C277 to serine fully disables the tRNA modification function of MnmG, as previously reported [31]. We cannot rule out the possibility that change R196D had a destabilizing effect on protein EcMnmG (1–550) under our ITC conditions since the interaction with EcMnmG(535–629) was completely abolished (Table 1), whereas the full-length EcMnmG-R196D protein produced a wild-type tRNA modification phenotype when overexpressed (Table 2). It should be noted that mutation R554D barely affected the affinity of EcMnmG(535–629) toward MnmE (Table 1; K_d = 43 μM, which represents a 1.7-fold increase respect to the control K_d value of 25 μM) supporting the idea that residue R554(548), like E585(579), is involved in the interaction of the C_{ARM} with the MnmG catalytic core, but not with MnmE. Notably, R554D also retarded the migration of the full-length EcMnmG protein in NRE gels (Fig. 5b), likely as a consequence of disruption of the salt bridge between R554(548) and residue D253(E260) of the other protomer (Fig. 2 and Supplementary Fig. 6).

Given that the AaMnmG form II crystal does not reveal any interaction of E585(579) or R554(548) with the rest of MnmG (Fig. 2a), our data suggest that EcMnmG can adopt in solution the form I conformation (Fig. 2b), which is physiologically relevant according to the tRNA modification analysis data.

Table 1. Validation of the C_{ARM} interactions with MnmE and the MnmG catalytic core using ITC

Cell	Syringe	K_d (μM)	*n*
MnmG(1–550)	MnmG(535–629)	1	0.96
MnmE	MnmG(535–629)	25	0.93
MnmG(1–550)	MnmG(535–629)E585K	21	0.81
MnmE	MnmG(535–629)E585K	24	0.91
MnmG(1–550)	MnmG(535–629)R554D	34	0.93
MnmE	MnmG(535–629)R554D	43	1.10
MnmG(1–550)D253R	MnmG(535–629)	26	1.10
MnmG(1–550)R196D	MnmG(535–629)	NB	–

Relative error in K_d is 20%–30%.
NB, no binding detected; *n*, binding stoichiometry.
Error in *n* is 0.1.

Oxidation of C277(284) as an strategy to stabilize a form-I open conformation

One important difference between the AaMnmG forms I and II involves the catalytic C277(284) residue [31,44]. In the AaMnmG form I, the C277(284)–C277 (284) intermolecular distance is much shorter (16 Å) than in the form II (57 Å) (Fig. 2 and Supplementary Fig. S9). Despite 16 Å being a large distance to form a disulfide bond, both C277(284) residues are facing each other, isolated from the solvent, and located in two large and flexible loops, which may allow a closer approach between them. Thus, we suspected that a disulfide bridge between the C277(C284) residues could be formed if EcMnmG adopts in solution the form I conformation (Fig. 2b). To test this hypothesis, proteins EcMnmG-WT, EcMnmG-C277S and EcMnmG-C47S were loaded onto a denaturing SDS-PAGE in

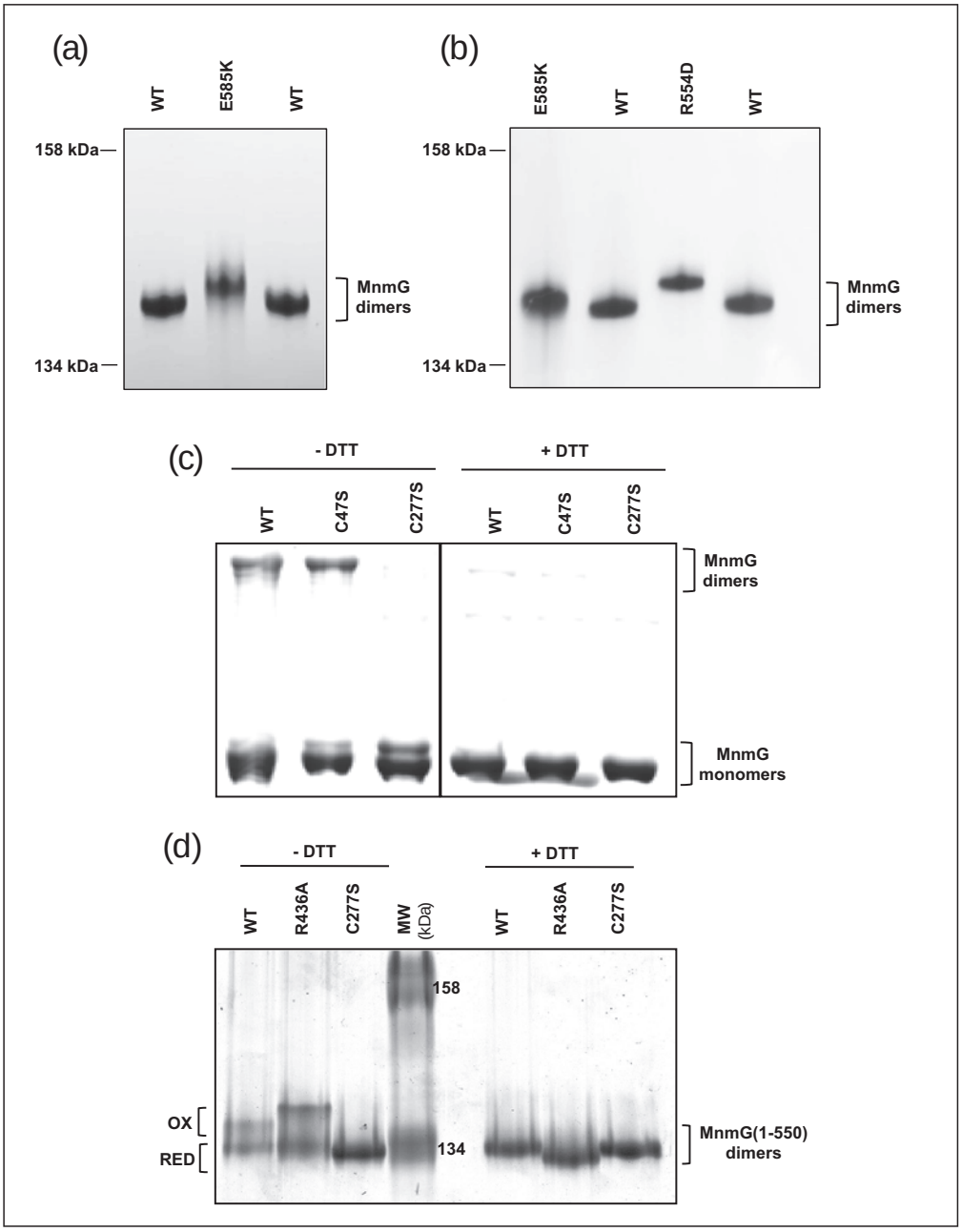

Fig. 5. Relevant intermolecular interactions in the AaMnmG form I. (a, b) NRE of reduced full-length MnmG and variants E585K (a and b) and R554D (b). (c) Effect of the C277S change on the formation of the interprotomer disulfide bridge. Protein samples were loaded onto a 6% SDS polyacrylamide gel in the presence or absence of DTT as indicated. (d) NRE of oxidized (OX) and reduced (RED) His-MnmG(1–550) variants under reducing (right panel) and non-reducing (left panel) electrophoretic conditions.

presence or absence of a reducing agent (50 mM DTT). C47 is a second catalytic residue that corresponds to AaMnmG C48 [31,44]. In the AaMnmG crystals, C48 is located at a distance of 3 Å from the isoalloxazine ring of FAD and 15 Å from the C284 of the same subunit, but the distance to any cysteine of the opposite protomer would be too long to form an intermolecular disulfide bridge (Supplementary Fig. S9). The EcMnmG proteins were treated with 20 mM of iodoacetamide prior to thermal denaturation and gel loading. The iodoacetamide irreversibly alkylates the free thiol groups of cysteines preventing any *de novo* disulfide bond formation during the manipulation of the samples [44,45]. As shown in Fig. 5c, mutation C277S, but not C47S, blocked the formation of the band representing the oxidized dimeric form of EcMnmG, indicating that the disulfide bridge established in the WT protein depends on C277 (C284 in AaMnmG). There are

Table 2. *In vivo* tRNA modification activity of MnmG variants

Strain/plasmid	MnmG protein	s^2U/s^4U ratio[a]	
		−ARA	+ARA
IC5241/pBAD22	None	0.026	0.030
IC5241/pIC1180	Flag-MnmG	0.009	0.000*
IC5241/pIC1793	Flag-MnmGR196D	0.026	0.000*
IC5241/pIC1794	Flag-MnmGD253R	0.026	0.000*
IC5241/ pIC1716	Flag-MnmGC277S	0.020	0.021
IC5241/pIC1795	Flag-MnmGR554D	0.026	0.000*
IC5241/pIC1440	Flag-MnmGE585K	0.019	0.006

[a] s^2U is the relevant modification that accumulates at position 34 of tRNAs when the MnmG function is impaired or suboptimal. Nucleoside s^4U at position 8 was used as an internal control. The numbers are calculated as the absorbance of s^2U relative to the absorbance of s^4U at 314 nm, and they are the mean from at least three independent experiments. The asterisks indicate that s^2U was undetectable. −ARA and +ARA indicate the absence or presence of the inducer arabinose in the growth medium.

two additional cysteines in EcMnmG, the partially conserved C242 (C249 in AaMnmG) and the non-conserved C418, which is substituted by a threonine in AaMnmG (T425), but their distance to C277(284) on the opposite protomer (inferred from the AaMnmG structure) is too long to establish disulfide bridges in native conditions (Supplementary Fig. S9). Altogether these data indicate that an intermolecular disulfide bridge through the C277(284) residues can be formed in EcMnmG, which supports the idea that EcMnmG in solution can adopt the form I conformation.

The AaMnmG form I structure suggests that residue R436(443), located in the FAD domain, may play a key role in the stabilization of the dimeric catalytic core of the protein by interacting with residue D289(296), located in the Ins-2 domain, of the opposite protomer (Fig. 2b). Notably, mutation R436A has been shown to abolish the tRNA modification activity of EcMnmG [31,32]. Thus, we set out to investigate the role of C277 (284) and R436(443) in the conformation of EcMnmG (1–550) by NRE [43], in the absence or presence of DTT. Under oxidizing conditions, retarded bands were detected in lanes corresponding to the EcMnmG (1–550)WT and EcMnmG(1–550)R436A proteins, but not in the lane corresponding to the EcMnmG(1–550) C277S variant (Fig. 5d, left). The retarded bands disappeared when the oxidized proteins were reduced with DTT (Fig. 5d, right). These data indicated that the retarded bands correspond to C277-dependent oxidized forms of the dimeric EcMnmG(1–550) variants, and that EcMnmG can adopt the dimerization interface of the form I structure even in the absence of the C_{ARMs}. The most retarded band of the oxidized EcMnmG (1–550)R436A protein (Fig. 5d, left) likely corresponds to a dimeric EcMnmG catalytic core linked through the C277 disulfide bond but in a more expanded conformation than in the EcMnmG(1–550) WT protein due to the lack of R436-mediated interaction(s).

A model of the MnmEG complex based on the MnmG form I

Two models of the MnmEG complex have been proposed so far on the basis of the crystal structures of MnmE and the MnmG form II conformation [29,33,34]. Our findings indicating that EcMnmG in solution can adopt the dimerization interface of the form I open a new insight into MnmE and MnmG interaction.

The structural analysis of the AaMnmG form I reveals the presence of an intermolecular cavity bottom-sealed by the flexible and highly conserved segment 259(266)–279(286) including C277(284) (Fig. 6a). It is noteworthy that the intermolecular space of the AaMnmG form I and the dimeric N-terminal domain of MnmE have similar dimensions (Supplementary Fig. S10). The intermolecular distances between the one-carbon donor molecules in MnmE (THF–THF: 24.5 Å) and between the FAD molecules in AaMnmG (FAD–FAD: 36.5 Å) are in a range that enables the interaction between the components of each THF–FAD pair simultaneously if the dimeric N-terminal domain of MnmE could enter into the MnmG molecular space through the cavity observed on the MnmG surface. If so, two catalytic centers could be formed at the same time in the MnmEG complex ($\alpha_2\beta_2$ heterotetramer) as a result of the interaction between the dimeric N-terminal domain of MnmE and the dimeric catalytic core of the MnmG form I.

Interestingly, an NMA of the AaMnmG form I, using *elNémo* web-server [41], discloses a high flexibility of all MnmG domains. The motion pattern involves an opening of the intermolecular cavity (through the separation of the FAD domains) and a concomitant mutual approach of the N_{ARM}s, with the Ins-2 domains (each containing the corresponding flexible loop 259(266)–279(286)) acting as a central axis (Fig. 6b, Supplementary Figs. S11a and S11b, and Videos S1 and S2). Notably, the Cα displacements of the FAD domains are more pronounced in an MnmG(1–550) model, suggesting that the C_{ARM}s, which are also interactors of MnmE ([29,32] and Table 1 in this work), may modulate the mobility of the FAD domains. Similar results were obtained in an NMA performed with iMODS (Supplementary Fig. S11c and Videos S3 and S4). Therefore, the analysis with both servers suggests that the AaMnmG form I can oscillate in a range of conformations which mainly differ in the aperture of the intermolecular cavity and the distance between the N_{ARM}s.

Our NRE data indicated that the formation of the intermolecular disulfide bridge C277(284)–C277 (284) stabilizes a form I-like conformation with a more expanded EcMnmG catalytic core (Fig. 5d left, compare WT and C277S lanes), which suggests that the intermolecular cavity is wider in the oxidized than in the reduced conformation. Therefore, we asked whether the oxidation/reduction state of the MnmG

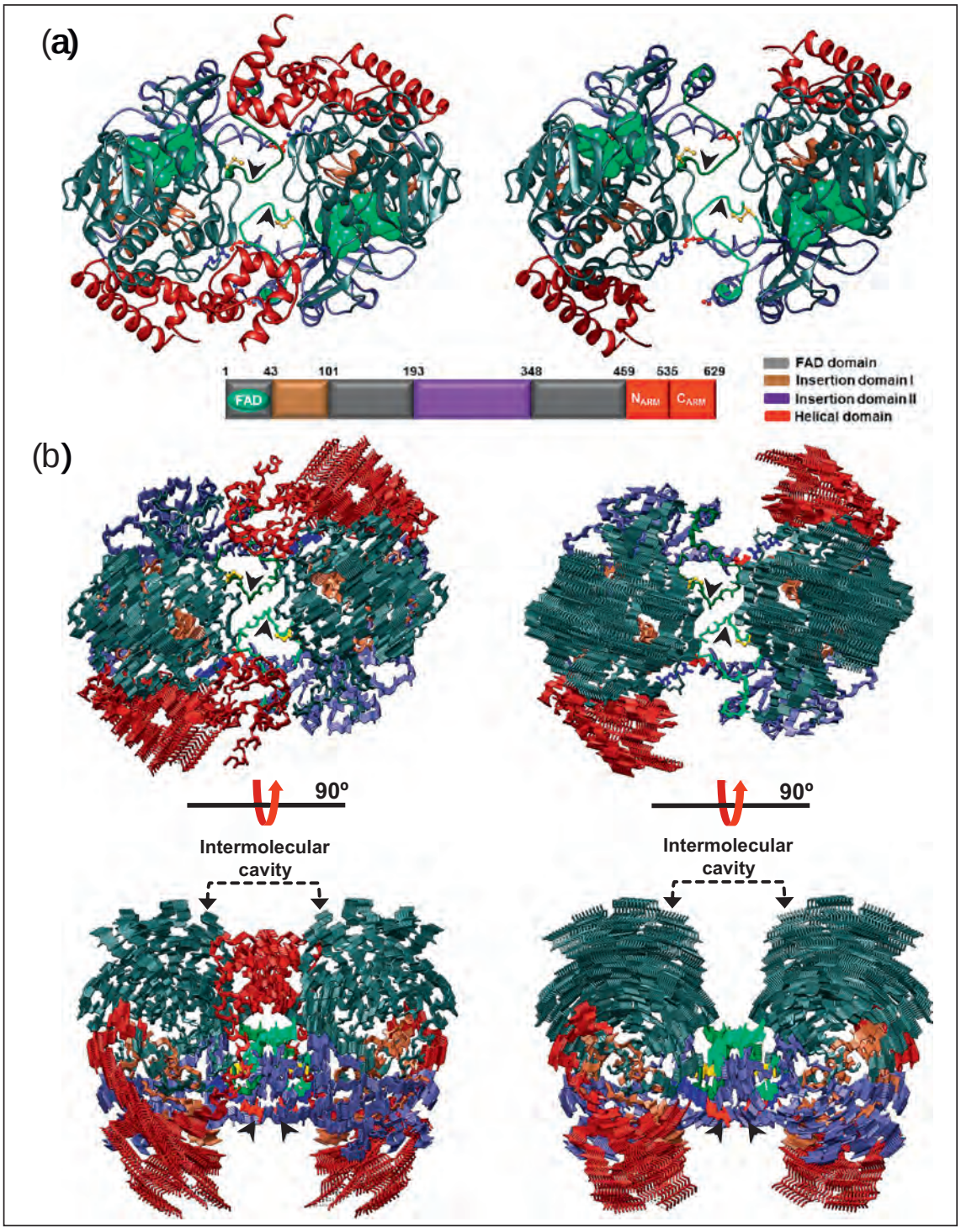

Fig. 6. Conformational dynamics of the MnmG form I computed from NMA. (a) Ribbon representation of the MnmG form I (left) and MnmG(1–550) (right) focused in the intermolecular cavity toward which the FAD molecules (green spheres) are oriented. Proteins are colored by domain (linear scheme) and the 259(266)–279(286) regions of each protomer are indicated by arrowheads and highlighted in dark and light green colors. Residues C277(284), R436(443) and D289(296) are represented in balls and sticks and colored in yellow, blue and red, respectively. (b) Backbone representation of the superposed normal mode intermediates of the MnmG form I (left) and MnmG(1–550) (right) performed by *elNémo* web server.

Table 3. ITC analysis of the ability of oxidized and reduced MnmG(1–550) variants to bind MnmE proteins

MnmG(1–550) protein	MnmE		MnmE(1–120)	
	K_d (μM)	*n*	K_d (μM)	*n*
MnmG(1–550)red	NB	–	NB	–
MnmG(1–550)ox	4.6	1.06	18	1.00
MnmG(1–550)C277Sox	47	0.93	ND	–
MnmG(1–550)R436Aox	26	0.92	ND	–
MnmG(1–550)C277Sred	>300	1.00	ND	–

Relative error in K_d is 20%–30%. Error in *n* is 0.1.
n, binding stoichiometry; red, reduced MnmG(1–550) protein; ox, oxidized MnmG(1–550) protein; NB, no binding observed; ND, not determined.

catalytic core could affect the binding to MnmE. As shown in Table 3 and Supplementary Fig. S12, only the oxidized form of protein EcMnmG(1–550) was able to interact with both the full-length EcMnmE protein and the EcMnmE(1–120) variant, while the reduced EcMnmG(1–550) protein bound neither EcMnmE, in agreement with previous reports [29,32], nor EcMnmE (1–120). Additional ITC experiments (Table 3 and Supplementary Fig. S12) revealed that the C277S change caused a substantial decrease in the affinity of oxidized EcMnmG(1–550) toward MnmE. These results support the idea that the MnmEG catalytic center may be formed through the interaction of the dimeric MnmE N-terminal domain and the dimeric catalytic core of MnmG adopting a form I conformation similar to the oxidized one.

We also observed that the oxidized EcMnmG (1–550)R436A exhibited a 5-fold decrease in the affinity toward MnmE in comparison with the oxidized EcMnmG(1–550)WT protein. This finding indicates that residue R436(443) plays a role in modulating the form I conformation that yields a proper MnmE interaction. Given the NRE pattern of oxidized EcMnmG(1–550) R436A (Fig. 5d, left), it is possible that an excessively open conformation of form I due to R436A weakens the MnmE binding. Finally, the fact that the oxidized EcMnmG(1–550)C277S protein exhibited higher affinity toward MnmE than the reduced EcMnmG(1–550) C277S protein suggests that oxidation of residues other than C277(C284) also contributes to stabilize open conformations of the form I.

tRNA docking model of the AaMnmG form I: A role for R436(439) and C277(284) in the interaction of MnmG with tRNA

Analysis of the surface electrostatic potential of the AaMnmG protomer revealed a positively charged patch, which includes highly conserved residues from Ins-1, Ins-2 and the helical domain, and where the deep groove containing the isoalloxazine ring of FAD is located [31]. In the dimeric AaMnmG form II, these positive patches are spatially separated suggesting the presence of two independent tRNA binding sites, one for each protomer (Supplementary Fig. S13, left panels). In contrast, in the AaMnmG form I, the positive patches of both protomers are clustered on the face containing the FAD tunnels (Supplementary Fig. S13, right panels), which open to the opposite face of the intermolecular cavity (Supplementary Fig. S13, compare top and bottom right panels). Based on these data, we manually docked the *E. coli* $tRNA^{Glu}$ (PDB ID: 2DER) into the AaMnmG form I generating a model of the tRNA:MnmG-form I complex (Fig. 7). In this model, the anticodon arms are lodged in the positive patch of MnmG, such that each anticodon loop is in close proximity to the isoalloxazine moiety of FAD. Notably, in the complex built with the AaMnmG form I, each protomer interacts with both tRNA molecules (Fig. 7a), whereas in the complex with form II, each protomer binds only to one tRNA molecule (Fig. 7c and d).

The positively charged region of each AaMnmG protomer includes the highly mobile segment comprising residues 259(266)–279(286), which contains most of the strictly conserved sequence P274(281)–E281 (288) and, therefore, the catalytic C277(284) (Fig. 8A, zoomed-in area). This loop makes a difference between the MnmG forms I and II since it is continuous and visible in the electron density maps of the form I, but it is partially disordered in the form II (Supplementary Fig. S14), thus indicating the structural flexibility of this area [31]. This region is also disordered in the structures of EcMnmG [29,32] and CtMnmG [29] (Supplementary Fig. S14), which adopt the dimerization interface of the AaMnmG form II. The flexible loop 259(266)–279(286) is stabilized in the AaMnmG form I by several interactions (Fig. 8A, zoomed-in area), including those established by the key residues C277 (284), with G273(280) or P274(281), and R436(443), with D289(296). Notably, the arrangement of the flexible loop in the form I structure determines the position of residues R275(282) and Y276(283), which construct the tunnel entrance to the FAD active center. The diameters of this tunnel (10 × 15 Å) are similar to the average diameter (12.5 Å) of the tRNA anticodon helix, which suggests that the tunnel could provide direct access of U34 to the FAD molecule during the modification reaction (Fig. 8A, zoomed-in area, and Supplementary Fig. S15, top panel). In the AaMnmG form II, the loop 259(266)–279(286) is not stabilized, so that the FAD tunnel entrance is not correctly formed and the isoalloxazine ring becomes more exposed to the solvent (Supplementary Fig. S15, bottom panel).

Fig. 7. tRNA docking models of the AaMnmG forms I and II. (a, b) Bottom (a) and front (b) views of the surface electrostatic potential map of the MnmG form I. (c, d) Front (c) and bottom (d) views of the surface electrostatic potential map of the MnmG form II. Two $tRNA^{Glu}$ molecules (in gold) were manually docked using Chimera in function of the positive charge distribution and the position of FAD molecules.

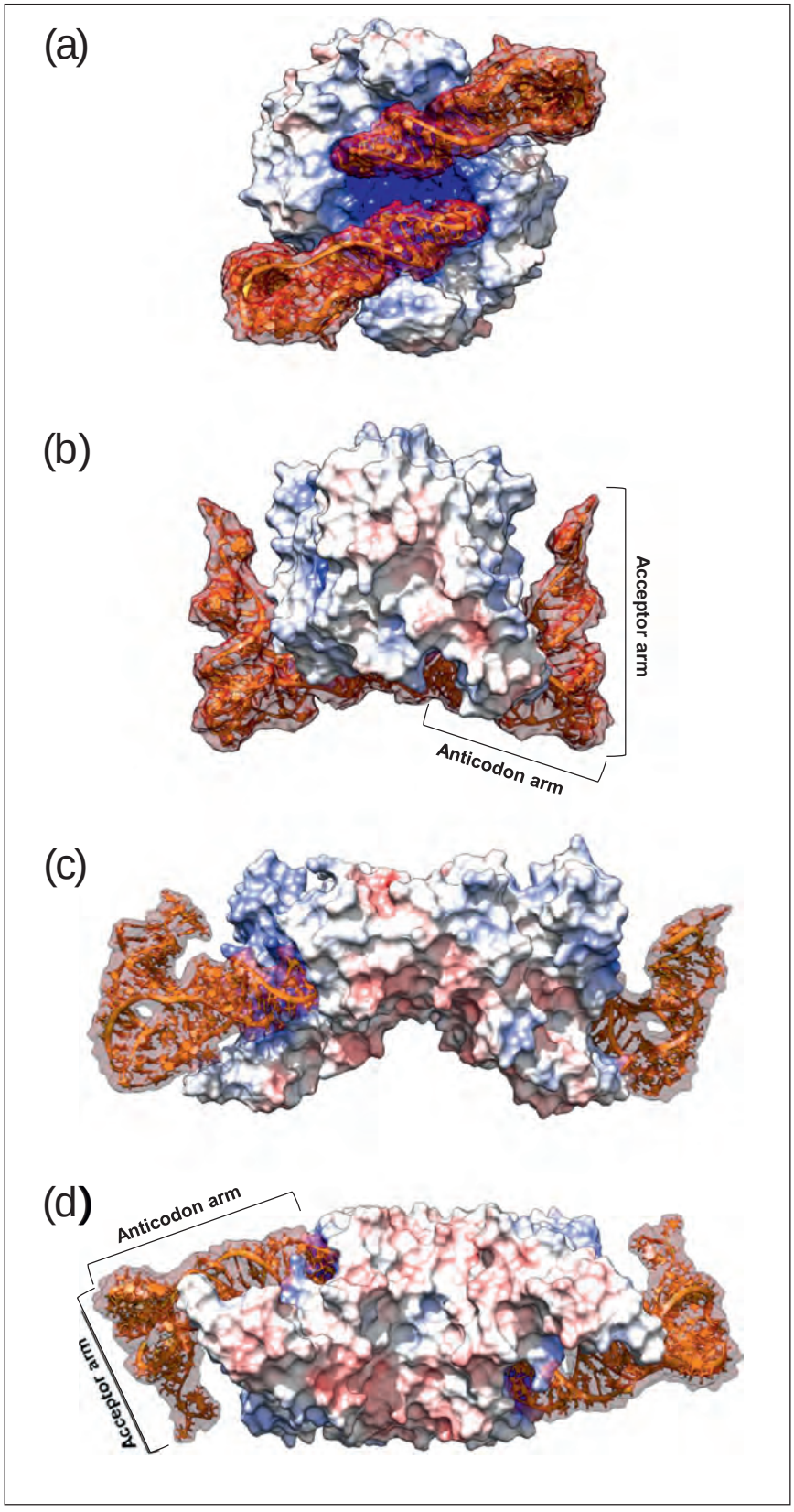

Fig. 7 (*legend on previous page*)

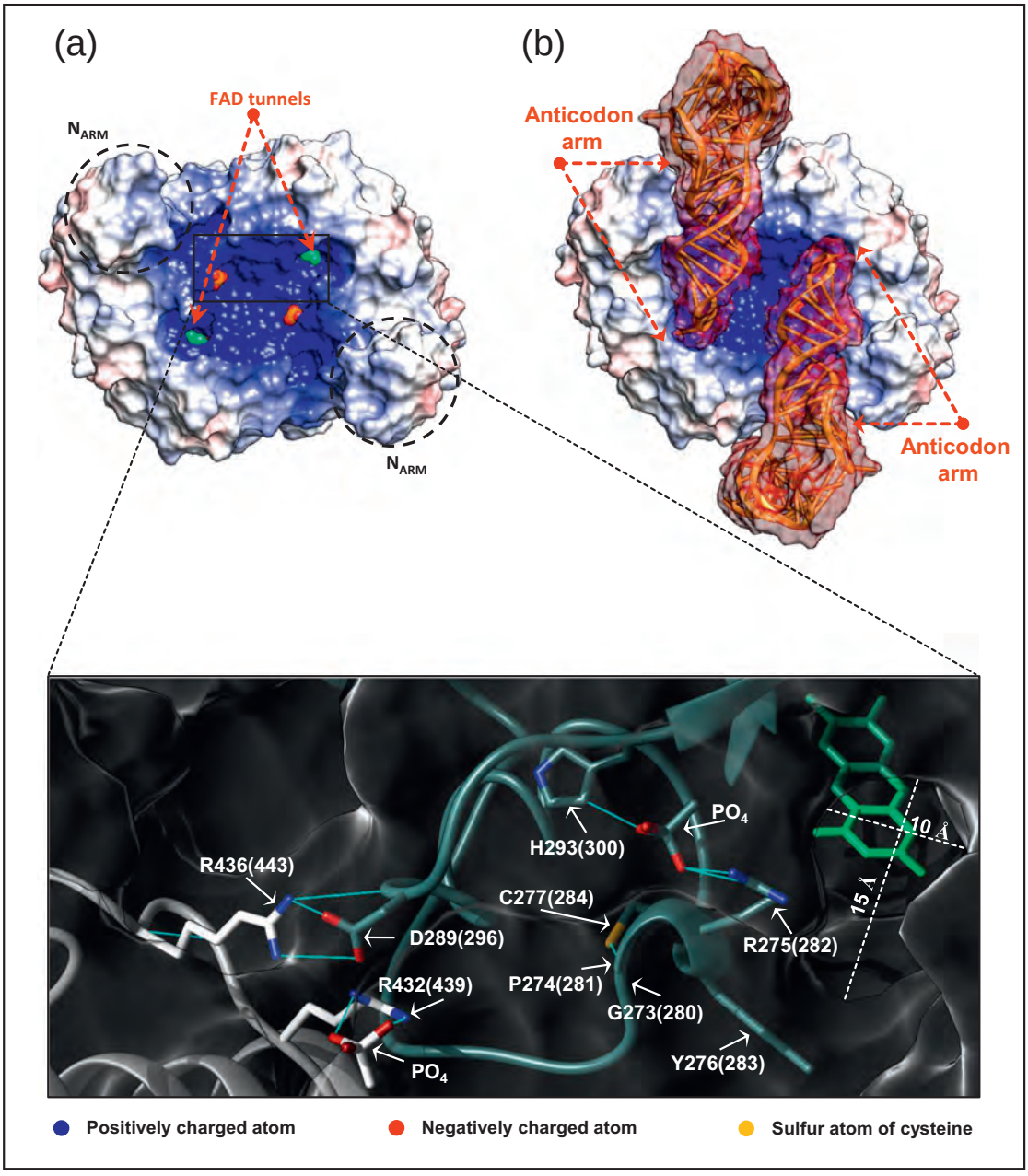

Fig. 8. The stabilization of the MnmG 259(266)–279(286) loop is required for the formation of the FAD tunnels. Bottom view of the electrostatic surface of the MnmG form I (a) with positively and negatively charged regions colored in blue and red, respectively. FAD and phosphate molecules are colored in green and dark magenta, respectively. Two $tRNA^{Glu}$ molecules (in gold) were manually docked using Chimera in function of the positive charge distribution and the position of FAD molecules (b). The bottom panel shows a zoomed-in view of the putative anticodon binding site. The 259(266)–279(286) region of one protomer (slate gray ribbon) becomes stabilized through several interactions described in the text, including those with the opposite protomer (white ribbon). The possible hydrogen bonds are colored in pale blue and the FAD isoalloxazine ring in green.

To experimentally test whether the EcMnmG residues C277(284) and R436(443) play a relevant role in the interaction with tRNA, we compared the migration pattern of the complexes formed between $tRNA^{Lys}$ and the wild-type or mutant versions of proteins EcMnmG and EcMnmG(1–550) by gel shift assays (electrophoretic mobility shift assay, or EMSA). There were no remarkable differences in the apparent affinity for $tRNA^{Lys}$ between the variants and the WT proteins (Fig. 9). However, the complexes of $tRNA^{Lys}$ with the variants R436A and C277S exhibited a striking increased mobility in relation to the complex with the WT controls (Fig. 9), suggesting that the R436A and C277S changes affect the manner in

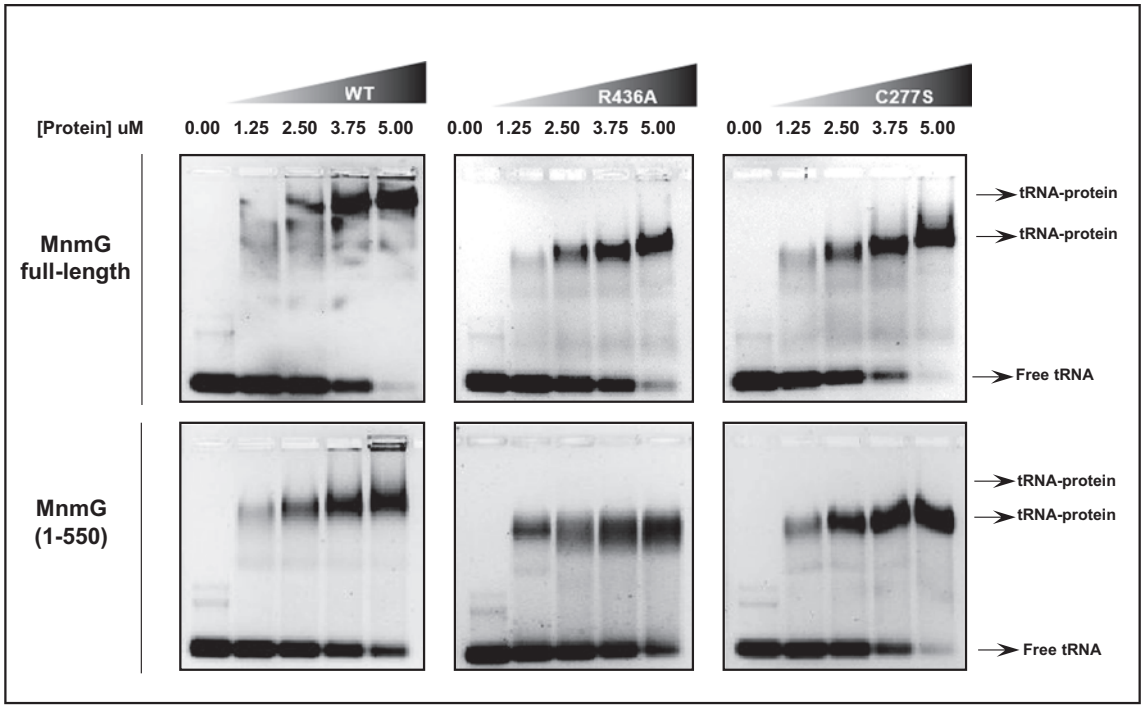

Fig. 9. EMSA of tRNA-MnmG complexes. *In vivo* overproduced $tRNA^{Lys}$ was incubated with increasing concentrations of His-MnmG full-length (upper panels) and His-MnmG(1–550) (lower panels) proteins (WT and variants R436A and C277S). Samples were loaded onto Tris–glycine–EDTA agarose gels, pre-stained with Gel Red.

which tRNA and EcMnmG interact, likely by preventing the stabilization of the flexible loop.

The C_{ARM} contains a SAM domain able to bind to tRNA

The positively charged patch of AaMnmG includes residues from the C_{ARM} region (Supplementary Fig. S13), suggesting that this region may also be involved in tRNA binding. In fact, it has been reported that a change of R554(548) to alanine weakened the affinity of the AaMnmG protein for tRNA and decreased the tRNA modification activity of EcMnmG [31]. Here, we found that protein EcMnmG(535–629) was able to bind both a substrate tRNA ($tRNA^{Lys}$) as well as a non-substrate tRNA ($tRNA^{Cys}$), suggesting that the C_{ARM} of the helical domain binds tRNA although non-specifically (Fig. 10a).

We used RBscore server [46] to predict RNA-binding residues from the AaMnmG C_{ARM}. Most of the identified residues are located in the E585(579)-containing face of the C_{ARM} (Fig. 10b), which suggests that this face can be involved in the interaction with the tRNA molecule, besides the MnmG catalytic core (Table 1).

The involvement of the C_{ARM} (residues 535–629 in EcMnmG) in diverse interactions together with the structural stability of this small region of the MnmG helical domain (Supplementary Fig. S4) prompted us to search for structural homologs. Interestingly, the DALI server [47], or the PDBeFold server [48], aligned the 560–618 region of AaMnmG with the SAM domains of recombinases Rad51 and RadA, the translational repressor Smaug, the helicase Hjm and the RNA polymerase (RpoA α-CTD) (Fig. 10c). Table 4 summarizes the proteins that were found to have the highest *Z*-scores according to the results obtained with DALI and PDBeFold. The SAM domains are characterized by their functional diversity (from signal transduction to transcriptional and translational regulation) despite adopting similar folds [49–52], but the MnmG C_{ARM} may be the first case reported of a SAM domain able to interact with tRNA.

Discussion

This work highlights the intricate conformational dynamics of MnmG, which is related to the tRNA modification process carried out by the MnmEG complex. We demonstrate that EcMnmG in solution, and in the absence of ligands, can adopt the dimerization interface of the form I crystal structure given that the formation of the C277(284) interprotomer disulfide bond is only compatible with form I-like conformations. Moreover, our data indicate that changes affecting the interaction of the C_{ARM} with the MnmG catalytic core, which only occurs if MnmG adopts the form I conformation, have a significant effect on both the migration of full-length MnmG

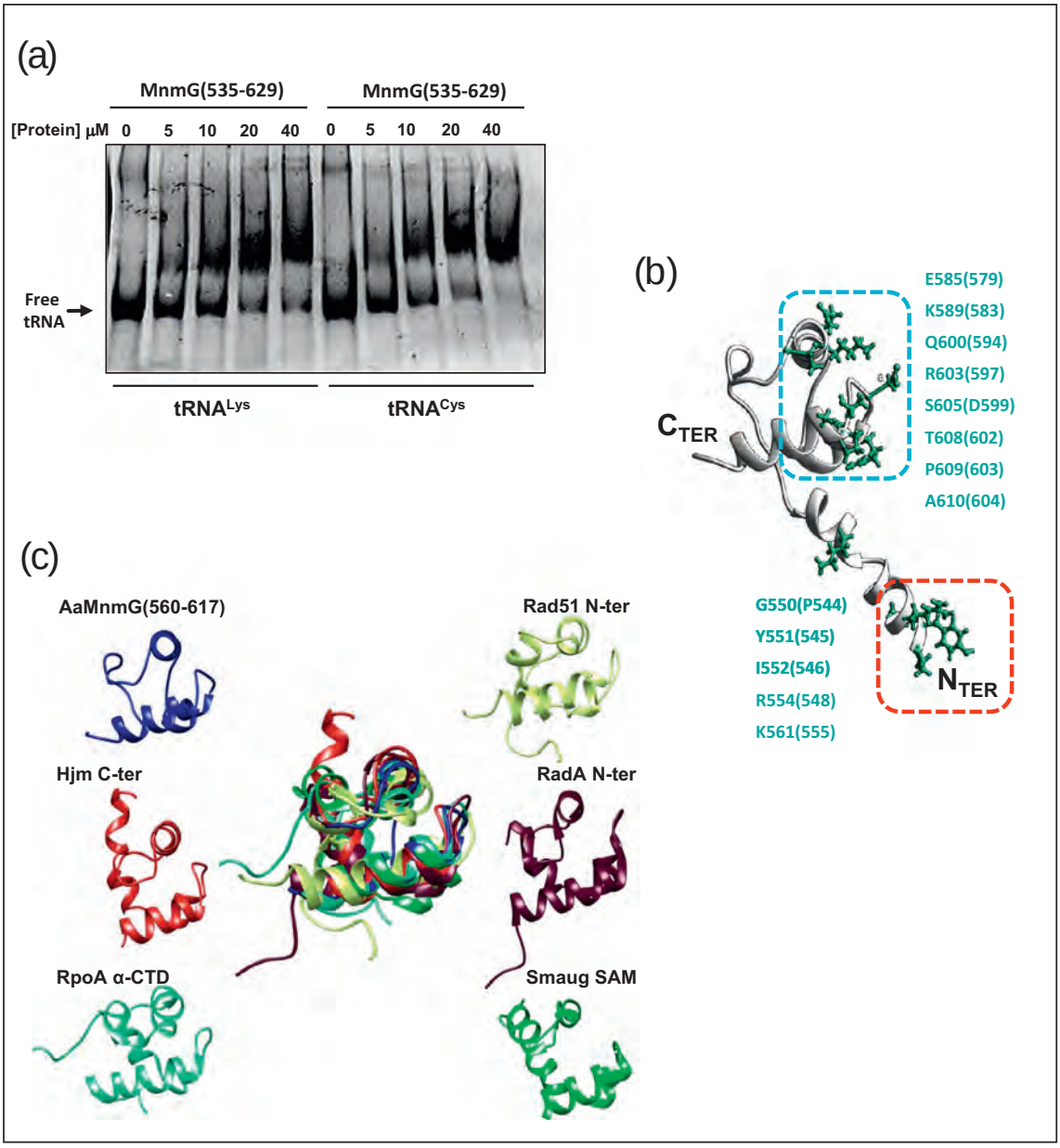

Fig. 10. The MnmG C_{ARM} contains a SAM domain capable to interact with tRNA. (a) Migration pattern of $tRNA^{Lys}$ and $tRNA^{Cys}$ in the absence or presence of increasing concentrations of the MnmG(535–629) protein. (b) Three-dimensional representation of the AaMnmG C_{ARM} highlighting residues predicted to interact with RNA, according to RBscore. (c) Ribbon representation of the SAM domains with high structural similarity with the 560–617 region of AaMnmG. Chimera superimposition of the SAM domains is shown in the central panel.

proteins and the biological activity of MnmG. We conclude, therefore, that the form I is physiologically relevant.

NMA supports the idea that form I can oscillate between open and closed conformations, with the Ins-2 domains (each containing the corresponding flexible 259(266)–279(286) loop) acting as a central axis (Fig. 6). Formation of the C277(284)–C277(284) intermolecular bond indicates that there has been a previous spatial approach of the two flexible loops, which is associated with a more open form-I conformation that is stabilized by the disulfide bridge (as indicated by the slower migration of the oxidized EcMnmG(1–550) protein in NRE). This expanded conformation entails an opening of the intermolecular cavity that facilitates the assembly of an MnmEG catalytic center mimic, since only oxidized MnmG (1–550)WT protein (and not the reduced one) is able to interact with the isolated THF-binding domain of MnmE or the full-length MnmE protein. The relative

Table 4. Proteins/Domains with structural homology to the region 560–617 of AaMnmG

Protein	PDB	RMSD[a]	*Z*[b]	N_{res}[c]	Sequence identity (%)	Function
Rad51	3LDA	2.1	5.0	49	24	Recombination
RadA	3ETL	2.3	4.9	49	22	Recombination
Hjm	2ZJ8	1.7	4.9	45	18	DNA repair
Smaug[d]	10XJ	2.5	4.4	37	22	Translation
RpoA	1DOQ	2.1	4.3	48	19	Transcription

[a] Root mean square deviation of superimposed C_α atoms calculated with DALI [47].
[b] *Z* score, computed by DALI (except those corresponding to Smaug), measures the statistical significance of a match in terms of Gaussian statistics. A *Z* score above 2 indicates structural similarity [47].
[c] Number of aligned residues.
[d] The data corresponding to the Smaug protein were computed with PDBeFold [48].

fast migration of the oxidized EcMnmG(1–550)C277S protein in NRE gels and the reduced affinity of this protein toward MnmE support the idea that formation of the C277(284)–C277(284) bond in the WT protein stabilizes a form-I open conformation able to bind MnmE. The finding that the oxidized EcMnmG(1–550) R436A protein exhibits the slowest migration in NRE gels and a 5-fold decrease in the affinity toward EcMnmG suggests that change R436A results in an excessively open conformation of form I that weakens the MnmE binding and leads to a non-functional MnmEG catalytic center, as the full-length EcMnmG-R436A protein is biologically inactive [31,32]. We conclude that only by adopting a proper expanded conformation, like the one stabilized by the C277–C277 disulfide bond and R436 interactions, the MnmG dimeric catalytic core can accept the entry of the dimeric THF-binding domain of MnmE into the FAD active center to assemble a functional MnmEG complex. Accordingly, an open conformation of the MnmG form I would be involved in the initial steps of the modification reaction.

The form I conformation adopted in the crystal structure (PDB ID: 2ZXH) represents an MnmG reduced protein. In this conformation, each C277 (284) is stabilizing its correspondent FAD tunnel entry, providing the hydrogen atom in an intraloop hydrogen bond with the main chain of G273(280) or P274(2829 (Fig. 8a, zoomed-in area). For the stabilization of the flexible loop 259(266)–279(286), and consequently of the FAD tunnel entry, the interaction of R436(443) with D289(296) on the opposite protomer is also required. Gel retardation experiments (in reducing conditions) showed the relevance of the C277(284) and R436 (443) residues in the tRNA–EcMnmG complex conformation (Fig. 9). These data suggest that a reduced MnmG form I is required for a functional access of the tRNA anticodon to the FAD active center. It is noteworthy that residue R436(443) appears to play a crucial role in the stabilization of the flexible loop in both the open (oxidized-like) and closed (reduced) conformation of form I.

Altogether our data suggest a model (Supplementary Fig. S16) in which the transition between open and closed states of the MnmG form I modulates key steps of the tRNA modification reaction. In this model, an open (oxidized-like) conformation would allow the access of the dimeric MnmE THF-binding domain to the MnmG FAD active center, facilitating the first steps of the reaction (i.e., those resulting in the formation of the group to be incorporated into U34), whereas the reduced (closed) conformation would be associated with the disengagement of the MnmE THF-binding domain from the MnmG intermolecular space and the entry of tRNA anticodons into the respective FAD tunnels. Then, the chemical group produced during the first part of the reaction could be incorporated to the position 5 of U34 [16]. There is wide evidence that the GTPase cycle of MnmE orchestrates the modification reaction [33,34,36,37,39], and that, in turn, MnmG induces large conformational and dynamic changes in MnmE, thus modulating its GTPase cycle [34,53]. Our data suggest that the C_{ARM}s may play a critical role in the communication between MnmE and the MnmG form I. In addition, formation of RNA–protein complexes usually involves conformational changes in the protein, the RNA, or both [54,55], and it has been shown that RNA molecules may modulate protein interactions [56]. Therefore, we suspect that the interactions of MnmG with MnmE and tRNA could modulate the dynamics of form I.

MnmG is paralogous of TrmFO, a folate/FAD-dependent methyltransferase that catalyzes the methylation of the C5-uridine 54 in the T-loop of tRNAs of most $Gram^+$ bacteria and some $Gram^-$ bacteria [57]. The structure of TrmFO reveals a monomeric protein consisting of a FAD domain and an insertion domain, but lacking the C-terminal helical domain present in MnmG [58]. TrmFO belongs to a class of folate-dependent methyltransferases that employ a flavin coenzyme for both the methylene and hydride transfer steps of the reaction [57]. In TrmFO, two catalytic cysteines (the nucleophile and the general base), which align perfectly with C277(284) and C47(48) of MnmG, have been proposed to work in concert during the methylation reaction [44,57,59]. MnmG could roughly follow the TrmFO mechanism, but with some

significant variations, given the higher complexity of the group to be added to the C5-uridine 34 (U34), and the indispensable participation of MnmE in the modification reaction. Unfortunately, no intermediates in the reaction mediated by the MnmEG complex have been identified so far; therefore, it is hard to propose a precise mechanism beyond the scheme illustrated in Supplementary Fig. S16 because it would be highly speculative. In any case, our data provide a view of how both the THF-binding domain of MnmE and the U34 of tRNA would gain a sequential alternative access to the FAD active center, thanks to the dynamics of the form I, which could be greatly modulated by the catalytic cycle of MnmEG. Adoption by the MnmG form I of open and closed conformations guarantees the formation of an isolated active center in which the reactants are all within short distances from the FAD.

The electrostatic surface potential exhibited by the form I and II conformations (Supplementary Fig. S13) together with our docking models (Fig. 7) prompt us to speculate that a transition from form I to form II could be involved in the release of the modified tRNA. However, this transition involves a reorientation of the protomers that requires breaking the R436-dependent link(s) and the interactions between the C_{ARM} and the MnmG catalytic core. Moreover, the form II conformation should then transit to the form I conformation in order to initiate a new modification cycle. We cannot rule out the possibility that the transition between forms I and II of MnmG is also driven by the dynamic interaction of MnmG with both MnmE and tRNA.

An additional finding of this work is the identification of a SAM domain in the C_{ARM} region, which is involved in the interaction with non-SAM domains (the MnmE helical domain and the MnmG catalytic core) and even with tRNA, thus playing crucial roles in the tRNA modifying process. Complexes of MnmG with MnmE and tRNA are, however, required to shed further light on the precise nature of these interactions.

In summary, the information reported in this study provides a dynamical view of the MnmG flavoenzyme and a new perspective to understand how a molecular machine like the MnmEG complex modifies tRNA.

Materials and Methods

Bacterial strains, plasmids, and DNA manipulations

E. coli strains and plasmids are listed in Supplementary Tables S1 and S2, respectively. For DNA manipulations, standard procedures were followed. Plasmids pIC1446, pIC1675 and pIC1614 were constructed by inserting the desired *mnmE* and *mnmG* sequences between the NdeI and XhoI sites of pET-15b. Plasmid pIC1574 was obtained by site-directed mutagenesis with appropriate primers in such a way that a stop codon was generated after residue 550 of MnmG. Derivatives from pIC1180, pIC1446, pIC1675 and pIC1574 were obtained by site-directed mutagenesis with appropriate primers.

tRNA manipulations and reverse-phase HPLC analysis of nucleosides

Purification of *E. coli* $tRNA^{Lys}$ expressed from pIC1664 was carried out in the *E.coli* strain DH5α as described previously [15]. Unmodified $tRNA^{Lys}$ and $tRNA^{Cys}$ were prepared by *in vitro* transcription from BstNI-digested plasmids pIC1083 and pIC1394, respectively, using the Riboprobe T7 transcription kit (PROMEGA) and 2–5 μg of each digested plasmid as a DNA template in a 50-mL reaction mix [15]. To study the effect of *mnmG* mutations on the tRNA modification status, the *E. coli* strain IC5241, an MG1655 derivative carrying the *mnmG::kan* allele [13], was transformed by pIC1180 and derived plasmids. Cells were grown in LB broth with thymine until the optical density at 600 nm (OD_{600}) reached 0.4. The culture was then divided into two equal parts, arabinose (0.2%) was added to one of them, and incubation was continued until OD_{600} reached 1.0. Cells were collected and processed for tRNA purification and Western blot analyses. It is noteworthy that in the absence of the inducer arabinose, wild-type levels of MnmG and its stable variants are produced because the pIC1180-based expression system is leaky [32]. Total tRNA purification and analysis of nucleosides by HPLC were performed as described previously [14]. The absorbance of nucleosides was monitored at 314 nm to maximize the detection of thiolated nucleosides. mnm^5s^2U (the final product of the MnmEG-dependent pathway) and s^4U (a nucleoside independent of the MnmEG pathway and used herein as a reference) were identified by their UV spectra and appropriate controls.

General protein techniques

For purification of His-tagged proteins, cells were grown in Luria-Bertani medium at 37 °C until OD reached 0.6–0.8. Protein overexpression was then induced by adding IPTG to a final concentration of 0.1 mM (0.25 mM for strains bearing pIC1675 and derivatives) for 16 h at 20° C. Cells were resuspended in buffer A [50 mM Tris–HCl (pH 7.5), 500 mM NaCl (or 250 mM NaCl for the His-MnmG (535–629) purification), 5 mM $MgCl_2$, 5 mM β-mercaptoethanol and 15 mM of imidazole] supplemented with 1 mM of phenylmethylsulfonyl fluoride, lysed by sonication and centrifuged at 40,000*g* for 30 min. The soluble fraction was incubated with TALON metal affinity resin (Clontech) for 1 h at 4 °C. After several washes with buffer A, proteins were eluted in buffer A supplemented with 250 mM of imidazole, concentrated by ultrafiltration using

Centricons (Amicon) with appropriated pore sizes and dialyzed in buffer A (in absence of β-mercaptoethanol and imidazole). Then, proteins were treated with 100 mM of DTT overnight at 4 °C. DTT was eliminated by ultrafiltration and the concentrated proteins were frozen in liquid nitrogen and stored at −80° until use. Monomeric and dimeric forms of MnmE(1–120) were obtained after the purification procedure. In this study, we used only the dimeric form, which was purified by size exclusion chromatography using a Superdex 75 column (GE Healthcare) in an AKTA Purifier FPLC (Amersham Biosciences). Expression and purification of GST-MnmE protein were performed as described previously [37]. The Flag-tagged MnmG proteins used in NRE assays were overexpressed and purified as described previously [13] with minor modifications. A concentration of 500 mM NaCl and 5 mM $MgCl_2$ was maintained during all steps of the purification procedure.

NRE

NRE was carried out as described previously [43] with some modifications. Protein samples, each containing 15 μg of protein in sample buffer [25 mM Tris–HCl (pH 7.5), 100 mM NaCl, 5 mM $MgCl_2$, 15 % glycerol and 0.02 % Red Ponceau 2S, with or without 20 mM DTT], were loaded onto 8% polyacrylamide gels prepared in 375 mM Tris–HCl (pH 8.8), 10% glycerol, 0.012% of Ponceau Red S. A solution of Tris–glycine (pH 8.8) with or without 0.012% Ponceau Red S was used as the cathode and anode buffer, respectively. Electrophoresis was performed at a constant current of 25 mA for 150–240 min at 4 °C. Finally, proteins were detected in gel using standard Coomassie Blue staining. The oxidized MnmG (1–550) proteins were obtained by dialyzing the purified proteins during 36 h at 4 °C with constant agitation in a 50 mM Tris–HCl (pH 7.5), 500 mM NaCl and 5 mM $MgCl_2$ buffer.

Detection of intermolecular disulfide bonds

MnmG proteins were purified as aforementioned but in the absence of reducing agents. Ten micrograms of purified His-MnmG protein (wild-type or mutant versions) was mixed with SDS sample buffer, containing DTT or not (50 mM), previously supplemented with 20 mM of iodoacetamide. Samples were thermally denatured and loaded onto a 6 % (w/v) SDS-PAGE. Proteins were detected in gel using standard Coomassie Blue staining.

EMSA

Capability of the MnmG(535–629) to bind tRNA was determined as follows: *In vitro* transcribed tRNA (5 μM final concentration) was incubated with increasing concentrations of His-MnmG(535–629) in binding buffer [Tris–HCl 25 mM (pH 7.5), 150 mM NaCl, 5 mM $MgCl_2$, 5 mM DTT and 20% glycerol] for 30 min at 4 °C. After incubation, the mixtures were electrophoresed in a 17% (w/v) Tris–glycine–EDTA polyacrylamide gel at a constant current of 30 mA for 210 min at 4 °C. Gels were stained with ethidium bromide and visualization was done in a standard UV transilluminator. The effect of mutations R436A and C277S on the migration of tRNA-MnmG or tRNA-MnmG(1–550) complexes was analyzed as follows: *In vivo* synthesized recombinant $tRNA^{Lys}$ (1.4 μM final concentration) was incubated with increasing concentrations of His-MnmG or His-MnmG(1–550) in binding buffer as above. Mixtures were run in a 1% (w/v) Tris–glycine–EDTA agarose gel, pre-stained with Gel Red (Invitrogen), at a constant current of 40 mA for 120 min at 4 °C. Gel visualization was done with a standard UV transilluminator.

ITC

ITC measurements were performed at 25 °C with an Auto-iTC200 isothermal titration calorimeter (MicroCal-Malvern) in a buffer consisting of 50 mM Tris–HCl (pH 7.5), 150 mM NaCl and 5 mM MgCl2, which was supplemented with 5 mM of β-mercaptoethanol except in the experiments with the oxidized forms of His-MnmG(1–550) or its variants. For binding measurements, a protein concentration in the cell and syringe of 20 μM and 200 μM, respectively, was used. To obtain the K_d values, the data were analyzed using nonlinear least-squares regression employing a model considering a single set of binding sites implemented in Origin 7.0 (OriginLab). The oxidized form of MnmG(1–550) was obtained as described in the "NRE" subsection. The presence of the oxidized dimeric form of His-MnmG(1–550) was monitored using NRE.

In silico protein analysis

Molecular graphics and analyses (interatomic distances, bond identification, structure superimpositions, etc.) were performed with the UCSF Chimera package [60]. The MnmG surface electrostatic potentials maps were calculated with the Adaptative Poisson–Boltzman solver implemented in Chimera package. Assembly analysis of the MnmG forms I and II and the identification of residues forming intermolecular hydrogen bonds in the MnmG form I (Fig. 2) were performed using the "Protein Interfaces Surface and Assemblies" service PDBePISA [42] at the European Bioinformatics Institute, (http://www.ebi.ac.uk/pdbe/prot_int/pistart.html). The identified residues were confirmed with Chimera package. Protein sequence alignment was performed with ClustalX [61] and edited with Jalview [62] coloring the sequence by conservation (Blosum62 matrix). In the rendering, by residue conservation, of protein structures with

Chimera, the same color scheme was used. NMAs were performed using *elNémo* (http://www.sciences.univ-nantes.fr/elnemo/) and iMODS (http://imods.chaconlab.org/) webservers [40,41]. The PDB ID of the input files used were 2ZXI and 2ZXH for the protomer and dimer NMA, respectively. All parameters were set to the default values with the exception of the amplitude. In *elNémo* analysis, the maximum amplitude (DQmax) was set to 250 arbitrary units for the MnmG form I dimer analysis. In the animations generated by iMODS, the amplitude was set to 5 and 4 arbitrary units for the MnmG full-length and MnmG (1–550), respectively, correlating with the length of the vectors represented.

Statistical analysis

Values are expressed as the mean of a minimum of three independent experiments with a standard deviation, unless otherwise specified.

Protein data bank accession numbers

MnmG *E. coli*: PDB ID: 3CES, 3CP2
MnmG *C. tepidum*: PDB ID: 3CP8
MnmG *A. aeolicus* (form II): PDB ID: 2ZXI
MnmG *A. aeolicus* (form I): PDB ID: 2ZXH
MnmE *C. tepidum*: PDB ID: 3GEE
MnmE *Nostoc* PDB ID: 3GEH
MnmE *T. maritima* PDB ID: 1XZP
$tRNA^{Glu}$ *E. coli*: PDB ID: 2DER

Supplementary data to this article can be found online at https://doi.org/10.1016/j.jmb.2018.05.035.

Acknowledgments

The authors thank Drs. E. Knecht, José L. Carrascosa, Jaime Martín-Benito and Rocío Arranz for their generous support to our research work, stimulating discussions and valuable comments on the manuscript. The authors also thank Dr. C. Navarro-González for valuable experimental assistance.

Funding: This work was supported by the Spanish Ministry of Economy and Competitiveness (BFU2010-19737 and BFU2014-58673-P to M.-E.A.; BFU2016-78232-P to A.V.-C.), and Generalitat Valenciana (ACOMP/2012/065 to M.-E.A; PROMETEO/2012/061 to J.B.). Funding for open access charge: [BFU2014-58673-P to M.-E.A.].

Conflict of Interest: None declared.

Received 25 April 2018;
Accepted 25 May 2018
Available online 2 June 2018

Keywords:
flavoenzymes;
interprotomer disulfide bridges;
MnmE;
MTO1;
sterile alpha motif

Abbreviations used:
AaMnmG, MnmG from *Aquifex aeolicus*; EcMnmG, MnmG from *Escherichia coli*; CtMnmG, MnmG from *Chlorobium tepidum*; U34, uridine 34; NRE, native red electrophoresis; EMSA, electrophoretic mobility shift assay; ITC, isothermal titration calorimetry; cmnm, carboxymethylaminomethyl group; nm, aminomethyl group; SAM, sterile alpha motif.

References

[1] P.C. Dedon, T.J. Begley, A system of RNA modifications and biased codon use controls cellular stress response at the level of translation, Chem. Res. Toxicol. 27 (2014) 330–337.
[2] H.-Y. Huang, A.K. Hopper, Multiple layers of stress-induced regulation in tRNA biology, Life 6 (2) (2016) 16.
[3] S. Kirchner, Z. Ignatova, Emerging roles of tRNA in adaptive translation, signalling dynamics and disease, Nat. Rev. Genet. 16 (2015) 98–112.
[4] M.E. Armengod, S. Meseguer, M. Villarroya, S. Prado, I. Moukadiri, R. Ruiz-Partida, et al., Modification of the wobble uridine in bacterial and mitochondrial tRNAs reading NNA/NNG triplets of 2-codon boxes, RNA Biol. 11 (2014) 1495–1507.
[5] B. El Yacoubi, M. Bailly, de Crécy-LagardV. , Biosynthesis and function of posttranscriptional modifications of transfer RNAs, Annu. Rev. Genet. 46 (2012) 69–95.
[6] T. Karlsborn, H. Tükenmez, A.F. Mahmud, F. Xu, H. Xu, A.S. Byström, Elongator, a conserved complex required for wobble uridine modifications in Eukaryotes, RNA Biol. 11 (2014) 1519–1528.
[7] S. Tsutomu, N. Asuteka, S. Takeo, Human mitochondrial diseases caused by lack of taurine modification in mitochondrial tRNAs, Wiley Interdiscip. Rev. RNA 2 (2011) 376–386.
[8] R. Schaffrath, S.A. Leidel, Wobble uridine modifications—a reason to live, a reason to die? RNA Biol. (2017) 1–14.
[9] W. Deng, I.R. Babu, D. Su, S. Yin, T.J. Begley, P.C. Dedon, Trm9-catalyzed tRNA modifications regulate global protein expression by codon-biased translation, PLoS Genet. 11 (2015), e1005706.
[10] D.D. Nedialkova, S.A. Leidel, Optimization of codon translation rates via tRNA modifications maintains proteome integrity, Cell 161 (2015) 1606–1618.
[11] B. Zinshteyn, W.V. Gilbert, Loss of a conserved tRNA anticodon modification perturbs cellular signaling, PLoS Genet. 9 (2013), e1003675.
[12] H. Cabedo, F. Macián, M. Villarroya, J.C. Escudero, M. Martínez-Vicente, E. Knecht, et al., The *Escherichia coli* trmE (mnmE) gene, involved in tRNA modification, codes for an evolutionarily conserved GTPase with unusual biochemical properties, EMBO J. 18 (1999) 7063–7076.
[13] L. Yim, I. Moukadiri, G.R. Björk, M.-E. Armengod, Further insights into the tRNA modification process controlled by proteins MnmE and GidA of *Escherichia coli*, Nucleic Acids Res. 34 (2006) 5892–5905.

[14] I. Moukadiri, S. Prado, J. Piera, A. Velázquez-Campoy, G.R. Björk, M. Armengod, Evolutionarily conserved proteins MnmE and GidA catalyze the formation of two methyluridine derivatives at tRNA wobble positions, Nucleic Acids Res. 37 (2009) 7177–7193.
[15] I. Moukadiri, M.-J. Garzón, G.R. Björk, M.-E. Armengod, The output of the tRNA modification pathways controlled by the *Escherichia coli* MnmEG and MnmC enzymes depends on the growth conditions and the tRNA species, Nucleic Acids Res. 42 (2014) 2602–2623.
[16] M.-E. Armengod, I. Moukadiri, S. Prado, R. Ruiz-Partida, A. Benítez-Páez, M. Villarroya, et al., Enzymology of tRNA modification in the bacterial MnmEG pathway, Biochimie 94 (2012) 1510–1520.
[17] H. Grosjean, M. Breton, P. Sirand-Pugnet, F. Tardy, F. Thiaucourt, C. Citti, et al., Predicting the minimal translation apparatus: lessons from the reductive evolution of mollicutes, PLoS Genet. 10 (2014), e1004363.
[18] V. de Crécy-Lagard, C. Marck, H. Grosjean, Decoding in *Candidatus Riesia pediculicola*, close to a minimal tRNA modification set? Trends Cell Mol. Biol. 7 (2012) 11.
[19] J.P. McCutcheon, N.A. Moran, Extreme genome reduction in symbiotic bacteria, Nat. Rev. Microbiol. 10 (2012) 13.
[20] A. Martínez-Zamora, S. Meseguer, J.M. Esteve, M. Villarroya, C. Aguado, J.A. Enríquez, et al., Defective expression of the mitochondrial-tRNA modifying enzyme GTPBP3 triggers AMPK-mediated adaptive responses involving complex i assembly factors, uncoupling protein 2, and the mitochondrial pyruvate carrier, PLoS One 10 (2015), e0144273.
[21] R. Boutoual, S. Meseguer, M. Villarroya, E. Martín-Hernández, M. Errami, M.A. Martín, et al., Defects in the mitochondrial-tRNA modification enzymes MTO1 and GTPBP3 promote different metabolic reprogramming through a HIF–PPARγ–UCP2–AMPK axis, Sci. Rep. 8 (2018) 1163.
[22] K. Asano, T. Suzuki, A. Saito, F.-Y. Wei, Y. Ikeuchi, T. Numata, et al., Metabolic and chemical regulation of tRNA modification associated with taurine deficiency and human disease, Nucleic Acids Res. 46 (2018) 1565–1583.
[23] E. Baruffini, C. Dallabona, F. Invernizzi, J.W. Yarham, L. Melchionda, E.L. Blakely, et al., MTO1 mutations are associated with hypertrophic cardiomyopathy and lactic acidosis and cause respiratory chain deficiency in humans and yeast, Hum. Mutat. 34 (2013) 1501–1509.
[24] D. Ghezzi, E. Baruffini, T.B. Haack, F. Invernizzi, L. Melchionda, C. Dallabona, et al., Mutations of the mitochondrial-tRNA modifier MTO1 cause hypertrophic cardiomyopathy and lactic acidosis, Am. J. Hum. Genet. 90 (2012) 1079–1087.
[25] R. Kopajtich, T.J. Nicholls, J. Rorbach, M.D. Metodiev, P. Freisinger, H. Mandel, et al., Mutations in GTPBP3 cause a mitochondrial translation defect associated with hypertrophic cardiomyopathy, lactic acidosis, and encephalopathy, Am. J. Hum. Genet. 95 (2014) 708–720.
[26] M. Villarroya, S. Prado, J.M. Esteve, M.A. Soriano, C. Aguado, D. Pérez-Martínez, et al., Characterization of human GTPBP3, a GTP-binding protein involved in mitochondrial tRNA modification, Mol. Cell. Biol. 28 (2008) 7514–7531.
[27] A. Scrima, I.R. Vetter, M.E. Armengod, A. Wittinghofer, The structure of the TrmE GTP-binding protein and its implications for tRNA modification, EMBO J. 24 (2005) 23–33.
[28] S. Meyer, S. Böhme, A. Krüger, H.-J. Steinhoff, J.P. Klare, A. Wittinghofer, Kissing G domains of MnmE monitored by X-ray crystallography and pulse electron paramagnetic resonance spectroscopy, PLoS Biol. 7 (2009), e1000212.
[29] S. Meyer, A. Scrima, W. Versees, A. Wittinghofer, Crystal structures of the conserved tRNA-modifying enzyme GidA: implications for its interaction with MnmE and substrate, J. Mol. Biol. 380 (2008) 532–547.
[30] T. Osawa, H. Inanaga, T. Numata, Crystallization and preliminary X-ray diffraction analysis of the tRNA-modification enzyme GidA from *Aquifex aeolicus*, Acta Crystallogr. Sect. F Struct. Biol. Cryst. Commun. 65 (2009) 508–511.
[31] T. Osawa, K. Ito, H. Inanaga, O. Nureki, K. Tomita, T. Numata, Conserved cysteine residues of GidA are essential for biogenesis of 5-carboxymethylaminomethyluridine at tRNA anticodon, Structure 17 (2009) 713–724.
[32] R. Shi, M. Villarroya, R. Ruiz-Partida, Y. Li, A. Proteau, S. Prado, et al., Structure–function analysis of *Escherichia coli* MnmG (GidA), a highly conserved tRNA-modifying enzyme, J. Bacteriol. 191 (2009) 7614–7619.
[33] M. Fislage, E. Brosens, E. Deyaert, A. Spilotros, E. Pardon, R. Loris, et al., SAXS analysis of the tRNA-modifying enzyme complex MnmE/MnmG reveals a novel interaction mode and GTP-induced oligomerization, Nucleic Acids Res. 42 (2014) 5978–5992.
[34] S. Meyer, A. Wittinghofer, VerséesW. , G-domain dimerization orchestrates the tRNA wobble modification reaction in the MnmE/GidA complex, J. Mol. Biol. 392 (2009) 910–922.
[35] M. Fislage, L. Wauters, W. Versées, Invited review: MnmE, a GTPase that drives a complex tRNA modification reaction, Biopolymers 105 (2016) 568–579.
[36] M. Martínez-Vicente, L. Yim, M. Villarroya, M. Mellado, E. Pérez-Payá, G.R. Björk, et al., Effects of mutagenesis in the switch I region and conserved arginines of *Escherichia coli* MnmE protein, a GTPase involved in tRNA modification, J. Biol. Chem. 280 (2005) 30660–30670.
[37] S. Prado, M. Villarroya, M. Medina, M.-E. Armengod, The tRNA-modifying function of MnmE is controlled by post-hydrolysis steps of its GTPase cycle, Nucleic Acids Res. 41 (2013) 6190–6208.
[38] A. Scrima, A. Wittinghofer, Dimerisation-dependent GTPase reaction of MnmE: how potassium acts as GTPase-activating element, EMBO J. 25 (2006) 2940–2951.
[39] L. Yim, M. Martínez-Vicente, M. Villarroya, C. Aguado, E. Knecht, M.-E. Armengod, The GTPase activity and C-terminal cysteine of the *Escherichia coli* MnmE protein are essential for its tRNA modifying function, J. Biol. Chem. 278 (2003) 28378–28387.
[40] J.R. Lopéz-Blanco, J.I. Garzón, P. Chacón, iMod: multipurpose normal mode analysis in internal coordinates, Bioinformatics 27 (2011) 2843–2850.
[41] K. Suhre, Y.-H. Sanejouand, ElNemo: a normal mode web server for protein movement analysis and the generation of templates for molecular replacement, Nucleic Acids Res. 32 (2004) (W610-W4).
[42] E. Krissinel, K. Henrick, Inference of macromolecular assemblies from crystalline state, J. Mol. Biol. 372 (2007) 774–797.
[43] T. Dráb, J. Kračmerová, I. Tichá, E. Hanzlíková, M. Tichá, H. Ryšlavá, et al., Native red electrophoresis—a new method suitable for separation of native proteins, Electrophoresis 32 (2011) 3597–3599.
[44] D. Hamdane, M. Argentini, D. Cornu, H. Myllykallio, S. Skouloubris, G. Hui-Bon-Hoa, et al., Insights into folate/FAD-dependent trna methyltransferase mechanism role of two highly conserved cysteines in catalysis, J. Biol. Chem. 286 (2011) 36268–36280.

[45] L. Tetsch, C. Koller, A. Dönhöfer, K. Jung, Detection and function of an intramolecular disulfide bond in the pH-responsive CadC of *Escherichia coli*, BMC Microbiol. 11 (2011) 74.
[46] Z. Miao, E. Westhof, Prediction of nucleic acid binding probability in proteins: a neighboring residue network based score, Nucleic Acids Res. 43 (2015) 5340–5351.
[47] L. Holm, C. Sander, Protein structure comparison by alignment of distance matrices, J. Mol. Biol. 233 (1993) 123–138.
[48] E. Krissinel, K. Henrick, Secondary-structure matching (SSM), a new tool for fast protein structure alignment in three dimensions, Acta Crystallogr. Sect. D Biol. Crystallogr. 60 (2004) 2256–2268.
[49] C.A. Kim, J.U. Bowie, SAM domains: uniform structure, diversity of function, Trends Biochem. Sci. 28 (2003) 625–628.
[50] F. Qiao, J.U. Bowie, The many faces of SAM, Sci. STKE 2005 (2005) (re7-re).
[51] D. Stapleton, I. Balan, T. Pawson, F. Sicheri, The crystal structure of an Eph receptor SAM domain reveals a mechanism for modular dimerization, Nat. Struct. Mol. Biol. 6 (1999) 44–49.
[52] C.D. Thanos, J.U. Bowie, p53 family members p63 and p73 are SAM domain-containing proteins, Protein Sci. 8 (1999) 1708–1710.
[53] S. Böhme, S. Meyer, A. Krüger, H.-J. Steinhoff, A. Wittinghofer, J.P. Klare, Stabilization of G domain conformations in the tRNA-modifying MnmE-GidA complex observed with double electron electron resonance spectroscopy, J. Biol. Chem. 285 (2010) 16991–17000.
[54] E. Seif, B.M. Hallberg, RNA–protein mutually induced fit. Structure of *Escherichia coli* isopentenyl-tRNA transferase in complex with tRNA (Phe), J. Biol. Chem. 284 (2009) 6600–6604.
[55] J.R. Williamson, Induced fit in RNA–protein recognition, Nat. Struct. Mol. Biol. 7 (2000) 834–837.
[56] L. Wang, M. Ciganda, N. Williams, Defining the RNA–protein interactions in the trypanosome preribosomal complex, Eukaryot. Cell 12 (2013) 559–566.
[57] D. Hamdane, H. Grosjean, M. Fontecave, Flavin-dependent methylation of RNAs: complex chemistry for a simple modification, J. Mol. Biol. 428 (2016) 4867–4881.
[58] H. Nishimasu, R. Ishitani, K. Yamashita, C. Iwashita, A. Hirata, H. Hori, et al., Atomic structure of a folate/FAD-dependent tRNA T54 methyltransferase, Proc. Natl. Acad. Sci. U. S. A. 106 (2009) 8180–8185.
[59] D. Hamdane, M. Argentini, D. Cornu, B.A. Golinelli-Pimpaneau, M. Fontecave, FAD/folate-dependent tRNA methyltransferase: flavin as a new methyl-transfer agent, J. Am. Chem. Soc. 134 (2012) 19739–19745.
[60] E.F. Pettersen, T.D. Goddard, C.C. Huang, G.S. Couch, D.M. Greenblatt, E.C. Meng, et al., UCSF Chimera—a visualization system for exploratory research and analysis, J. Comput. Chem. 25 (2004) 1605–1612.
[61] M.A. Larkin, G. Blackshields, N. Brown, R. Chenna, P.A. McGettigan, H. McWilliam, et al., Clustal W and Clustal X version 2.0, Bioinformatics 23 (2007) 2947–2948.
[62] A.M. Waterhouse, J.B. Procter, D.M. Martin, M. Clamp, G.J. Barton, Jalview Version 2—a multiple sequence alignment editor and analysis workbench, Bioinformatics 25 (2009) 1189–1191.